

## Self-interaction correction in multiple scattering theory

M. Lüders,<sup>1</sup> A. Ernst,<sup>2</sup> M. Däne,<sup>3,1</sup> Z. Szotek,<sup>1</sup> A. Svane,<sup>4</sup> D. Ködderitzsch,<sup>3,1</sup> W. Hergert,<sup>3</sup> B. L. Györfy,<sup>5</sup> and W. M. Temmerman<sup>1</sup>

<sup>1</sup>*Daresbury Laboratory, Daresbury, Warrington, WA4 4AD, United Kingdom*

<sup>2</sup>*Max Planck Institut für Mikrostrukturphysik, Weinberg 2, D-06120 Halle, Germany*

<sup>3</sup>*Fachbereich Physik, Martin-Luther-Universität Halle-Wittenberg, Friedemann-Bach-Platz 6, D-06099 Halle, Germany*

<sup>4</sup>*Institute of Physics and Astronomy, University of Aarhus, DK-8000 Aarhus, Denmark*

<sup>5</sup>*H. H. Wills Physics Laboratory, University of Bristol, Tyndall Avenue, Bristol BS8 1TL, United Kingdom*

(Received 24 June 2004; revised manuscript received 1 February 2005; published 19 May 2005)

We propose a simplified version of self-interaction corrected local spin-density (SIC-LSD) approximation, based on multiple scattering theory, which implements self-interaction correction locally, within the KKR method. The multiple scattering aspect of this new SIC-LSD method allows for the description of crystal potentials which vary from site to site in a random fashion and the calculation of physical quantities averaged over ensembles of such potentials using the coherent potential approximation. This facilitates applications of the SIC to alloys and pseudoalloys which could describe disordered local moment systems, as well as intermediate valences. As a demonstration of the method, we study the well-known  $\alpha$ - $\gamma$  phase transition in Ce, where we also explain how SIC operates in terms of multiple scattering theory.

DOI: 10.1103/PhysRevB.71.205109

PACS number(s): 71.10.-w, 64.70.Kb, 71.15.Ap, 71.15.Mb

### I. INTRODUCTION

The self-interaction corrected local spin density (SIC-LSD) approximation<sup>1,2</sup> has proved to be a useful scheme to describe static correlations in strongly correlated electron systems. In particular, it can determine whether an electron is delocalized or localized, i.e., whether its orbital is part of the valence states or not. This leads to a determination of the number of valence states and a nominal valence, as demonstrated by numerous calculations on rare earths, actinides, transition metal oxides, including the parent compounds of the high  $T_c$  materials and the CMR materials.<sup>3-9</sup>

The full SIC-LSD scheme is unfortunately difficult to implement.<sup>10</sup> This is due to the repeated transformations from reciprocal space ( $k$  space) to real space to evaluate the self-interaction potential and the back transformations to  $k$  space to solve the band structure problem. So far most applications of the full SIC-LSD formalism have been implemented in the LMTO-ASA (linearized muffin-tin orbitals in the atomic sphere approximation) band structure method.<sup>11</sup> In this paper a simpler but more versatile scheme is developed and implemented within multiple scattering theory, in the Korringa, Kohn, Rostocker (KKR) formulation. Its main advantage, thanks to a straightforward determination of the Green's function, is a possible generalization to alloys via the coherent potential approximation (CPA).<sup>12-16</sup> Since a single-site approximation underpins this new formulation, in what follows it is referred to as a local self-interaction correction (LSIC) formalism. It is based on the experience with the full SIC-LSD implementation showing that to better than 98% the electron is localized on the site under consideration, which justifies the single-site approximation. While in the full LMTO-ASA implementation, the representation of the localized orbitals over a real-space cluster determines the extent of these orbitals, in the present scheme the degree of localization is determined by the energy dependence of the single-site phase shift, in particular the width of its reso-

nance, corresponding to the localized electron. A broader resonance would imply reduced localization.

The SIC-LSD formalism for solids has been developed into a scheme that treats both localized and delocalized electrons on equal footing. The decision whether an electron should be considered as localized or delocalized is based on a delicate balance between the energy gain due to the inclusion of the self-interaction correction (localization) energy and the energy loss in band or hybridization energy.<sup>3</sup> While this methodology has been successful in differentiating localized from delocalized electrons, i.e., a dual character of the electron, it does not describe the interesting crossover between localized and delocalized states which occurs, for example, in heavy fermion systems. Our aim here is to develop a theory which describes local fluctuations of the electronic configurations between that where an electron can be said to be localized and another where an electron is delocalized. It will be shown that the present local formulation of SIC-LSD readily lends itself to be the basic idea of such a development. The origin of our approach goes back to the invention and use of the coherent potential approximation to describe the charge and spin fluctuations about the Hartree-Fock solution of the Hubbard model by Hubbard himself (Hubbard III approximation).<sup>17-19</sup> The present implementation of this idea rests on its generalization to account for the corresponding fluctuations about the local density approximation (LDA) to the first-principles density functional theory (DFT).<sup>20-22</sup> In the literature this generalization, when applied to spin fluctuations, is referred to as the KKR-CPA implementation of the disordered local moment (DLM) picture.<sup>23,24</sup> Indeed, the present work can be considered as the further elaboration of this basic idea in which the LSIC replaces the LDA as the local description of the electronic structure and the attention is being focused on the valence fluctuations. Interestingly, it is now well established that Hubbard's so-called "alloy analogy" approximation, which prompted the use of the CPA, leaves out of consideration some very important fluctuations.

The most significant of these are those which give rise to a Kondo-like resonance at the Fermi energy in the case of the Hubbard model and correspond to such a qualitatively new physics as the Mott transition. The relevance of this in the present context is that such fluctuations are well described by the dynamical mean field theory (DMFT)<sup>25</sup> whose static limit, for the Hubbard model, is precisely the “alloy analogy” CPA of Hubbard.<sup>19</sup> This point was particularly clearly explained in the recent paper of Kakehashi.<sup>26</sup> Consequently, it is reasonable to regard our LSIC based KKR-CPA-DLM calculations as investigations of the static limit of a yet undeveloped first principles DMFT. In what follows when we refer to the need to include dynamical effects in the theory it is the above theoretical considerations we will have in mind.

The paper is organized as follows. In Sec. II we outline the physical picture underlying the present approach. In Sec. III a general formulation of SIC-LSD, following Perdew and Zunger,<sup>1</sup> is briefly summarized with reference to some aspects of the LMTO-ASA implementation based on the Wannier function representation of localized orbitals.<sup>10</sup> In Sec. IV, the formalism of the local self-interaction corrected local spin density (LSIC-LSD) within multiple scattering theory is described in detail. There we concentrate on the phase shifts and single-site Green’s function from which the SIC charge and potential, corresponding to localized electron states, are calculated within the KKR method. Since the latter can be easily extended to include coherent potential approximation, Sec. V briefly summarizes its most important equations in terms of the multiple scattering quantities. In Sec. VI the formalism is extended to finite temperatures. The potential and versatility of the LSIC method is demonstrated on the application to the  $\alpha$ - $\gamma$  phase transition in Ce. In Sec. VII we first discuss the  $f$ -phase shifts, total energies, lattice parameters, densities of states (DOS), and spectral functions at  $T=0$  K for the  $\alpha$  and  $\gamma$  phases, as obtained from the LSIC-KKR method. Wherever appropriate we compare with the results of the full SIC-LSD implementations within LMTO-ASA.<sup>10</sup> In this section we also present calculations for finite temperatures and the full phase diagram of the  $\alpha$ - $\gamma$  phase transition. Both the CPA and DLM are utilized to accomplish the latter, and to illustrate how the present approach is capable to describe both spin and valence fluctuations at finite temperatures. Section VIII is devoted to various aspects of the present approach and among them a consideration of how intermediate valence could be realized within the present implementation, which motivates a possible generalization to include dynamics, as outlined in Sec. IX. The paper is summarized in Sec. X.

## II. PHYSICAL PICTURE

In the present formulation of SIC, we adopt the physical picture of multiple-scattering theory, where a solid is represented by an array of nonoverlapping scattering centers. The electronic motion is then broken down into a sequence of scattering events and a free propagation in between. The most useful concept of this method is a phase shift, describing scattering of electrons from ions, the scattering centers in a solid. If a phase shift is resonant it is reminiscent of a

bound state at positive energies, i.e., above the zero of the potential which in our case is the muffin-tin zero. The energy derivative of the phase shift is related to the Wigner delay time. If this is large the electron will spend a long time on the site. Such slow electrons will be much more affected by the spurious self-interaction and therefore should see a SI-corrected potential.

In most systems, where the electrons are truly delocalized, the self-interaction contribution to the potential is negligible and therefore the LDA is an excellent approximation. When the phase shift has a resonance one has to calculate the self-interaction correction for this  $(l, m)$  angular momentum channel. This is accomplished by calculating the one-electron charge density for this channel, defining the charge density for the self-interaction correction. From this one can readily calculate the self-interaction potential which has to be added to the LSD potential, and then the new phase shifts are calculated for the total (SIC-LSD) potential. This has to be carried out  $m$  channel by  $m$  channel for a given angular momentum  $l$ . The minimum of the total energy will determine the optimum configuration of  $(l, m)$  channels to be self-interaction corrected. Therefore to each of the  $m$  channels one can assign two potential functions,  $V_{\text{eff}}^{\text{SIC-LSD}}(r)$  and  $V_{\text{eff}}^{\text{LSD}}(r)$ . The formalism determining the energy functional associated with the potential  $V_{\text{eff}}^{\text{SIC-LSD}}(r)$  is briefly outlined in the next section. It should be mentioned here that if the total energies corresponding to these two different potentials are sufficiently close, one can envisage dynamical effects to play an important role as a consequence of possible tunneling between these states. We shall return to this point in the later sections.

## III. SIC-LSD FORMALISM

It has been pointed out by Perdew and Zunger<sup>1</sup> that density functional theory (DFT) schemes, like the local spin density approximation, suffer from a spurious self-interaction of the electrons with themselves. In principle, this self-interaction term should vanish exactly, as it does in the Hartree-Fock theory. In practice, however, this cancellation is incomplete. Perdew and Zunger suggested an approximate solution to this problem, which was constructed for finite systems but is here extended to solids in a different way as compared to previous implementations for solids.<sup>2</sup>

The usual representation of the total energy within the LSD-DFT formalism in the Kohn-Sham approach<sup>21</sup> is

$$E^{\text{LSD}}[n_{\uparrow}, n_{\downarrow}] = \sum_{\alpha\sigma}^{\text{occ}} \langle \phi_{\alpha\sigma} | -\nabla^2 | \phi_{\alpha\sigma} \rangle + E_{\text{ext}} + E_{\text{H}}[n] + E_{\text{xc}}^{\text{LSD}}[n_{\uparrow}, n_{\downarrow}], \quad (1)$$

where  $\phi_{\alpha\sigma}$ ’s are the Kohn-Sham orbitals [ $\alpha\sigma$  is a combined index labeling the orbital and spin ( $\uparrow$  or  $\downarrow$ ), respectively],  $n_{\alpha\sigma} = |\phi_{\alpha\sigma}|^2$ ,  $n_{\sigma} = \sum_{\alpha}^{\text{occ}} n_{\alpha\sigma}$ ,  $n = n_{\uparrow} + n_{\downarrow}$ .  $E_{\text{ext}}$  is the external field energy functional,  $E_{\text{H}}$  is the Hartree energy

$$E_H[n] = \int d^3r \int d^3r' \frac{n(\mathbf{r})n(\mathbf{r}')}{|\mathbf{r}-\mathbf{r}'|}, \quad (2)$$

and  $E_{xc}^{\text{LSD}}$  is the LSD approximation to the exchange-correlation energy functional. On the basis of the above, Perdew and Zunger proposed a self-interaction corrected LSD on an orbital by orbital basis

$$E^{\text{SIC-LSD}}[\{n_{\alpha\sigma}\}] = E^{\text{LSD}}[n_{\uparrow}, n_{\downarrow}] - \sum_{\alpha\sigma}^{\text{occ}} (E_H[n_{\alpha\sigma}] + E_{xc}^{\text{LSD}}[n_{\alpha\sigma}, 0]), \quad (3)$$

by subtracting explicitly the self-Coulomb and self-exchange and self-correlation energy of all *occupied* orbitals. This correction restores the property that the true functional  $E[n]$  should have, namely that the self-Coulomb energy exactly cancels the self-exchange and self-correlation energy for every single orbital,  $E_H[n_{\alpha\sigma}] + E_{xc}^{\text{exact}}[n_{\alpha\sigma}, 0] = 0$ . This leads to an orbital dependent SIC potential seen by an electron in orbital  $\phi_{\alpha\sigma}$ ,

$$V_{\text{eff},\alpha\sigma}^{\text{SIC-LSD}}(\mathbf{r}) = \underbrace{V_{\text{ext}}(\mathbf{r}) + V_H[n](\mathbf{r}) + V_{xc,\sigma}^{\text{LSD}}[n_{\uparrow}, n_{\downarrow}](\mathbf{r})}_{V_{\text{eff},\sigma}^{\text{LSD}}(\mathbf{r})} - \underbrace{V_H[n_{\alpha\sigma}](\mathbf{r}) + V_{xc,\sigma}^{\text{LSD}}[n_{\alpha\sigma}, 0](\mathbf{r})}_{V^{\text{SIC}}(\mathbf{r})}, \quad (4)$$

with the external lattice potential  $V_{\text{ext}}(\mathbf{r})$ , and

$$V_H[n](\mathbf{r}) = 2 \int d^3r' \frac{n(\mathbf{r}')}{|\mathbf{r}-\mathbf{r}'|}, \quad (5)$$

$$V_{xc,\sigma}^{\text{LSD}}[n_{\uparrow}, n_{\downarrow}](\mathbf{r}) = \frac{\delta E_{xc}^{\text{LSD}}[n_{\uparrow}, n_{\downarrow}]}{\delta n_{\sigma}}. \quad (6)$$

This self-interaction correction vanishes exactly only for extended states. In order to apply the SIC scheme to solids, the approach by Perdew and Zunger has to be generalized. This involves simultaneously a Wannier representation of the orbitals, necessary to determine  $n_{\alpha\sigma}$  of Eq. (4), and a Bloch representation to solve the band structure problem. Furthermore, the Wannier functions are required to fulfill the localization criterion which ensures that the energy functional is stationary with respect to unitarian mixing among the orbitals. This localization criterion is necessary, because the SIC is not invariant under unitary transformations of the occupied orbitals. This is in contrast with the LSD where a unitary transformation of the occupied orbitals leaves the LSD potential invariant, since the total charge density remains unaltered. For the orbital dependent SIC potential  $V^{\text{SIC}}$  such a unitary transformation will change  $V^{\text{SIC}}$ . The localization criterion  $\langle \alpha | V_{\alpha}^{\text{SIC}} - V_{\beta}^{\text{SIC}} | \beta \rangle = 0$  determines the unitary transformation which ensures the global minimum of the total energy and the hermiticity of the Hamiltonian. Solutions of this equation usually take the form of the eigenvector  $|\alpha\rangle$  having weight in one channel only  $[(\text{Im } \alpha_j)^2 + (\text{Re } \alpha_j)^2 = 1]$  which would be different from the channel where the weight of the eigenvector  $|\beta\rangle$   $[(\text{Im } \beta_j)^2 + (\text{Re } \beta_j)^2 = 1]$  is concentrated, i.e.,  $i$  is not equal to  $j$ . This generalization forms the basis of the

SIC implementations<sup>10,27</sup> which start from a band-picture scenario.

#### IV. SINGLE-SITE SIC-LSD FORMALISM

As already mentioned, the proposed generalization of the Perdew and Zunger idea is based on the notion of resonances in scattering theory, which are the reminiscence of atomic states in the solid. Core states are represented by bound states at negative energies, where the imaginary part of the generalized complex phase shift jumps abruptly by  $\pi$ . Localized valence states still have very sharp resonances but band-like states are characterized by slowly varying phase shifts.

The central quantity of (scalar-relativistic) multiple scattering theory is the single-particle Green's function<sup>15</sup>

$$G_{\sigma}(\mathbf{r}, \mathbf{r}'; \epsilon) = \sum_{LL'} \bar{Z}_{L\sigma}^i(\mathbf{r}_i; \epsilon) \tau_{\sigma LL'}^{ij}(\epsilon) Z_{L'\sigma}^j(\mathbf{r}'_j; \epsilon) - \sum_L \bar{Z}_{L\sigma}^i(\mathbf{r}_{<}; \epsilon) J_{L\sigma}^i(\mathbf{r}_{>}; \epsilon) \delta_{ij}, \quad (7)$$

with  $\mathbf{r} = \mathbf{R}_i + \mathbf{r}_i$ , where  $\mathbf{r}_i$  is a vector inside the cell at  $\mathbf{R}_i$ ,  $L = (l, m)$  denotes the combined index for the decomposition into symmetrized lattice harmonics  $Y_L$  and  $\mathbf{r}_{<}(\mathbf{r}_{>})$  is the vector smaller (larger) in magnitude from the pair  $(\mathbf{r}, \mathbf{r}')$ . The building blocks of the Green's function are the regular and irregular solutions of the radial Schrödinger equation at a given (complex) energy  $\epsilon$ ,

$$Z_{L\sigma}^i(\mathbf{r}_i; \epsilon) = Z_{l\sigma}^i(r_i; \epsilon) Y_L(\hat{\mathbf{r}}_i), \quad (8)$$

$$\bar{Z}_{L\sigma}^i(\mathbf{r}_i; \epsilon) = Z_{l\sigma}^i(r_i; \epsilon) Y_L^*(\hat{\mathbf{r}}_i), \quad (9)$$

$$J_{L\sigma}^i(\mathbf{r}_i; \epsilon) = J_{l\sigma}^i(r_i; \epsilon) Y_L(\hat{\mathbf{r}}_i). \quad (10)$$

The scattering-path matrix  $\underline{\tau}$  (in  $iL, jL'$  and  $\sigma$  representation),

$$\underline{\tau}(\epsilon) = [\underline{t}^{-1}(\epsilon) - \underline{g}(\epsilon)]^{-1} \quad (11)$$

is related to the structural Green's function  $\underline{g}(\epsilon)$ , describing the free propagation between the scattering centers, and the  $\underline{t}$  matrix defines the single-site scattering.

The total valence charge density per spin  $\sigma$  is given by

$$n_{\sigma}(\mathbf{r}) = -\frac{1}{\pi} \int_{E_B}^{E_F} d\epsilon \text{Im } G_{\sigma}(\mathbf{r}, \mathbf{r}; \epsilon), \quad (12)$$

where  $E_B$  and  $E_F$  denote the bottom of the valence band and the Fermi energy, respectively. In standard LSD calculations, the new effective potential for the next iteration of the self-consistency cycle is calculated from this density (now including the core contributions) as

$$V_{\text{eff},\sigma}^{\text{LSD}}(\mathbf{r}) = V_{\text{ext}}(\mathbf{r}) + V_H[n](\mathbf{r}) + V_{xc,\sigma}^{\text{LSD}}[n_{\uparrow}, n_{\downarrow}](\mathbf{r}). \quad (13)$$

In order to remove the spurious self-interaction, still present in this potential, we consider the problem of electrons moving in an array of scatterers. As already mentioned, an electron which shows localized behavior has a sharp resonance in its phase shift, associated with a large Wigner delay time

on a particular site. To determine the SIC charge we will consider for a moment the atomic limit, i.e., the situation where the scatterers are far apart. In this case the single-site  $t$  matrix and the local multiple scattering  $\tau$  matrix coincide, and all occupied states correspond to bound states. In this limit each bound state contributes exactly the charge of one electron, and this charge can be calculated by integrating the diagonal of the spectral function just around the energy of the bound state. In order to be able to decompose the charge density [Eq. (12)] into different angular momentum channels, we choose symmetry adapted spherical harmonics. These are defined by applying a unitary transformation to the ordinary real (or complex) spherical harmonics, such that the on-site scattering matrix becomes diagonal,

$$\sum_{L_1, L_2} U_{LL_1}^\dagger \tau_{L_1, L_2}^{ii}(\epsilon) U_{L_2 L'} = \delta_{LL'} \tilde{\tau}_{LL}^{ii}(\epsilon). \quad (14)$$

It is easy to verify that the required transformation matrix  $U$  is, in fact, independent of the energy  $\epsilon$ . This transformation to symmetry adapted spherical harmonics also ensures that the degeneracy of states, which are localized, is conserved. We will demonstrate this later by SI correcting the triplet states (one by one) of the Ce  $f$  manifold. In this symmetrized representation, the Green's function, which in the atomic limit equals the atomic Green's function, becomes diagonal with respect to this quantum number. Hence we can decompose the spin resolved charge density into its  $L$  components and define the charge of a state, characterized by its principle quantum number  $n$ , angular momentum  $L$ , and spin  $\sigma$ ,

$$n_{nL\sigma}^{\text{SIC}}(\mathbf{r}) = -\frac{1}{\pi} \int_{E_1}^{E_2} d\epsilon \text{Im} G_{LL,\sigma}(\mathbf{r}, \mathbf{r}; \epsilon), \quad (15)$$

where the energies  $E_1$  and  $E_2$  lie slightly below and above the energy of the state  $nL\sigma$ . Within the multiple scattering formulation, in the atomic limit, this charge density can be written as

$$n_{iL\sigma}^{\text{SIC}}(\mathbf{r}) = -\frac{1}{\pi} \int_{E_1}^{E_2} d\epsilon \text{Im} [\tilde{Z}_{L\sigma}^i(\mathbf{r}; \epsilon) \tau_{\sigma LL}^{ii}(\epsilon) Z_{L\sigma}^i(\mathbf{r}; \epsilon) - \tilde{Z}_{L\sigma}^i(\mathbf{r}; \epsilon) J_{L\sigma}^i(\mathbf{r}; \epsilon)], \quad (16)$$

where  $i$  is the site index, since in this case the single-site  $t$  matrix and the  $\tau$  matrix are obviously identical. This, of course, is not the case for a solid with finite lattice spacings. When considering resonances in a solid it is not *a priori* clear whether to use the  $t$  or  $\tau$  matrix for calculating the charge density in question. The main difference between using the  $t$  matrix or  $\tau$  matrix is that the latter does include a small hybridization of the localized state with the surrounding atoms, while the former does not. Also the choice of the lower and upper integration limits is not clearly defined. We will now give a short discussion of the possible modes for calculating the SIC charge of a resonant state.

The lower integration limit is most reasonably chosen to be the bottom of the energy contour  $E_B$ . However, care has to be taken that this contour always encloses the SI-corrected states. In the case of Ce, discussed in the following sections, the contour also includes the  $5p$  semicore states. The upper

integration limit could be either chosen such that the SIC charge density integrates to exactly one electron, or simply set to the Fermi energy  $E_F$ . Using the  $t$  matrix, we find that we have to integrate up to an  $E_{\text{top}}$ , which is slightly above the Fermi level in order to capture one electron. The  $\tau$  matrix, on the other hand, due to hybridization, yields a charge of one for energies slightly below the Fermi energy. Unfortunately, when dealing with the  $\tau$  matrix, it is computationally very expensive to assume  $E_2$  different from the Fermi energy. However, the excess charge due to integrating up to the Fermi level is only of the order of a hundredth of an electron. (The missing charge in case of integrating the  $t$  matrix up to the Fermi level is of similar magnitude.) In the following we used the  $\tau$  matrix integrated up to  $E_F$  to determine the SIC charge. Some tests with the  $t$  matrix, and the requirement of a SIC charge of unity, resulted in an upward shift of the total energies by about 1 mRy.

The charge density, calculated in either of the proposed ways, is used to construct the effective self-interaction free potential, namely

$$V_{\text{eff},iL\sigma}^{\text{SIC-LSD}}(\mathbf{r}) = V_{\text{eff},\sigma}^{\text{LSD}}(\mathbf{r}) - V_{\text{H}}[n_{iL\sigma}^{\text{SIC}}](\mathbf{r}) - V_{\text{xc}}^{\text{LSD}}[n_{iL\sigma}^{\text{SIC}}, 0](\mathbf{r}). \quad (17)$$

In this paper we only consider the spherically symmetric part of the SIC density and SIC potential. Hence, the  $t$  matrix is diagonal in  $l$  and  $m$ . Here it should be noted that, if we transform the equations back to the unsymmetrized (real or complex) spherical harmonics, this effective potential assumes matrix character with respect to the angular momentum, and would not simply couple to the density, but rather to the nondiagonal  $lm, l'm'$  density matrix. This is conceptually analogous to the rotationally invariant formulation of LDA+U by Dudarev *et al.*<sup>28</sup>

For each self-interaction corrected channel  $\tilde{L}=(\tilde{l}, \tilde{m})$  and  $\tilde{\sigma}$ , we replace the  $\tilde{L}th$  element of the original  $t$  matrix by the one obtained from the SI-corrected potential

$$\tilde{t}_{L\sigma}^i = t_{L\sigma}^i (1 - \delta_{L,\tilde{L}} \delta_{\sigma,\tilde{\sigma}}) + t_{L\sigma}^{i,\text{SIC-LSD}} \delta_{L,\tilde{L}} \delta_{\sigma,\tilde{\sigma}}, \quad (18)$$

where  $t_{L\sigma}^i$  is the  $t$  matrix calculated from the effective potential  $V_{\text{eff},\sigma}^{\text{LSD}}(\mathbf{r})$ , and  $t_{L\sigma}^{i,\text{SIC-LSD}}$  is calculated from the SI-corrected potential  $V_{\text{eff},iL\sigma}^{\text{SIC-LSD}}(\mathbf{r})$ . This  $\tilde{t}$  matrix is then used in Eq. (11) to calculate the SI-corrected scattering path matrix  $\tilde{\tau}$ . From the latter the new SIC-LSD charge density is calculated, and the process is iterated until self-consistency is reached. The correction term, which approximately compensates the self-repulsion, is an attractive potential which will pull down in energy the state to which it is applied (see Sec. VII).

To finish this section we would like to mention that in contrast to the LSD, the SIC-LSD Hamiltonian is not invariant under unitary transformations of the occupied orbitals. As pointed out before, in the full implementation the localization criterion is applied to make the solution stationary under this unitary mixing of states. In the present implementation there is no such localization criterion, and one has to be solely guided by the energetics to find the global energy minimum. Note that the total energies are invariant under a rotation of the coordinate system owing to the symmetry

adapted spherical harmonics that diagonalize the  $\tau$  matrix at the  $\Gamma$  point. Hence, the energies of the configurations where, one by one, each state out of a degenerate manifold is localized are the same. This was tested on Ce by SI correcting all  $f$  states separately. As expected, the energies for localizing any of the  $T_{1u}$  (or, respectively, the  $T_{2u}$ ) states were identical.

### V. CPA GENERALIZATION

One of the advantages of the multiple scattering implementation of the SIC-LSD formalism is that it can be easily generalized to include the coherent potential approximation,<sup>12-16</sup> extending the range of applications to random alloys. In addition, one can use it to treat static correlations beyond LSD by studying pseudoalloys whose constituents are composed, e.g., of two different states of a given system, one delocalized, described by the LSD potential, and another localized, corresponding to the SIC-LSD potential. Combined with the DLM formalism for spin fluctuations,<sup>23,24</sup> this allows also for different orientations of the local moments of the constituents involved.

In the CPA extension of the SIC-LSD formalism, bearing in mind its single-site aspect, it is required to satisfy the following CPA self-consistency condition

$$c\tau^{A,00}(\epsilon) + (1-c)\tau^{B,00}(\epsilon) = \tau^{C,00}(\epsilon), \quad (19)$$

where the impurity  $\tau$  matrices  $\tau^{A,00}(\epsilon)$  and  $\tau^{B,00}(\epsilon)$  are given by

$$\tau^{A,00}(\epsilon) = \frac{\tau^{C,00}(\epsilon)}{\{1 + \tau^{C,00}(\epsilon)[\underline{t}_A(\epsilon) - \underline{t}_C(\epsilon)]\}} \quad (20)$$

$$\tau^{B,00}(\epsilon) = \frac{\tau^{C,00}(\epsilon)}{\{1 + \tau^{C,00}(\epsilon)[\underline{t}_B(\epsilon) - \underline{t}_C(\epsilon)]\}}, \quad (21)$$

and the  $\tau$  matrix of the coherent potential approximation

$$\tau^{C,00}(\epsilon) = \frac{1}{\Omega_{\text{BZ}}} \int d^3k \frac{1}{[\underline{t}_C^{-1}(\epsilon) - \underline{g}(\vec{k}, \epsilon)].} \quad (22)$$

Here  $\Omega_{\text{BZ}}$  is the volume of the Brillouin zone (BZ),  $\underline{t}_A(\epsilon)$  and  $\underline{t}_B(\epsilon)$  are the respective single site scattering matrices of the  $A$  and  $B$  species, occurring with the concentrations  $c$  and  $1-c$ , respectively, and  $\underline{t}_C(\epsilon)$  is the  $t$  matrix of the effective CPA medium. Note that in the CPA extension of the SIC-LSD formalism, the CPA condition [Eq. (19)] is an additional self-consistency criterion to the usual charge or potential self-consistency.

Finally, it should be mentioned that the formalism of this section can be easily generalized from a binary to a multi-component case, as described in Ref. 29. In addition, an extension of the LSIC-CPA formalism to finite temperatures can be implemented as described in Sec. VI.

### VI. FINITE TEMPERATURES

In this section we summarize the relevant formulas underlying the finite temperature generalization of the present formalism in its CPA extension. In contrast to  $T=0$ , at finite

temperatures the physics is dominated by thermal (classical) fluctuations. Therefore, to properly take into account the finite temperature effects, one needs to evaluate the free energy of the system (alloy) under consideration, namely

$$F(T, c, V) = E_{\text{tot}}(T, c, V) - T[S_{\text{el}}(T, c, V) + S_{\text{mix}}(c) + S_{\text{mag}}(c) + S_{\text{vib}}(c)], \quad (23)$$

where  $S_{\text{el}}$  is the electronic (particle-hole) entropy,  $S_{\text{mix}}$  the mixing entropy,  $S_{\text{mag}}$  the magnetic entropy, and  $S_{\text{vib}}$  the entropy originating from the lattice vibrations.

The electron-hole entropy is defined as<sup>37</sup>

$$S_{\text{el}}(T, c, V) = -k_B \int d\epsilon n(\epsilon) \{f_{\beta}(\epsilon) \ln f_{\beta}(\epsilon) + [1 - f_{\beta}(\epsilon)] \ln [1 - f_{\beta}(\epsilon)]\}, \quad (24)$$

where  $k_B$  is the usual Boltzmann constant and  $f_{\beta}(\epsilon)$  denotes the Fermi-Dirac distribution function. The entropy of mixing in the case of a binary system can be expressed as

$$S_{\text{mix}}(c) = -k_B [c \ln c + (1-c) \ln (1-c)]. \quad (25)$$

The magnetic and vibrational entropies are strongly dependent on the system under consideration, and they will be discussed in more detail in the section dedicated to the phase diagram of Ce.

Finally, note that in the definition of the free energy, the finite temperature enters only via the Fermi-Dirac distribution and the entropy contributions, while for the exchange-correlation energy, being part of the total energy  $E_{\text{tot}}$ , the  $T=0$  K LDA (LSD) approximation is used for all temperatures, which is a common practice in all *ab initio* calculations.

This section completes the formal description and implementation of the LSIC-KKR-CPA band structure method. In the following sections we shall illustrate the potential and versatility of this approach for describing strongly correlated electron systems by an application to Ce. There we present both the  $T=0$  K and finite temperature results, including the phase diagram of the famous  $\alpha$ - $\gamma$  phase transition.

### VII. CE $\alpha$ - $\gamma$ PHASE TRANSITION

Ce is the first element in the periodic table that contains an  $f$  electron, and shows an interesting phase diagram.<sup>30</sup> In particular, its isostructural (fcc  $\rightarrow$  fcc)  $\alpha$ - $\gamma$  phase transition is associated with a 15%–17% volume collapse and quenching of the magnetic moment.<sup>30</sup> The low-pressure  $\gamma$  phase shows a local magnetic moment, and is associated with a trivalent configuration of Ce. At the temperatures in which the  $\gamma$  phase is accessible, it is in a paramagnetic disordered local moment state. Increasing the pressure, the material first transforms into the  $\alpha$  phase, which is indicated to be in an intermediate valence state with quenched magnetic moment. At high pressures (50 kbar at room temperature) Ce eventually transforms into the tetravalent  $\alpha'$  phase. With increasing temperature, the  $\alpha$ - $\gamma$  phase transition shifts to higher pressures, ending in a critical point (600 K, 20 kbar), above which there is a continuous crossover between the two phases.

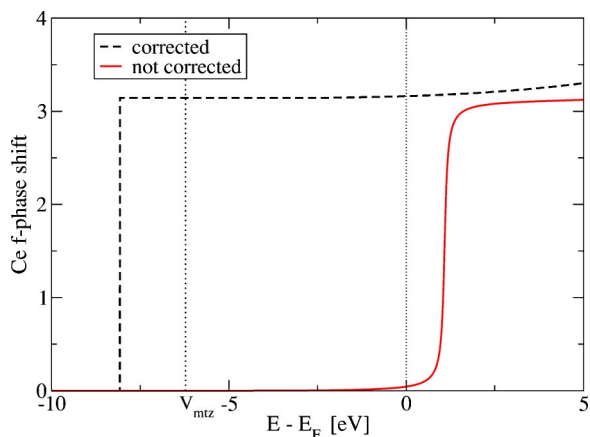


FIG. 1. (Color online) Phase shifts of the SI-corrected and uncorrected  $f$  states in Ce from the SIC-LSD calculation. The energies are relative to the Fermi level.

In the following paragraphs we first discuss the SIC and non-SIC  $f$ -phase shifts and densities of states. Then we compare the results of LSIC total energies, for the ferromagnetic arrangement of local moments, with the earlier calculations of the full SIC implementation, in order to benchmark the method. After discussing the density of states of the LDA and SIC-LSD calculations, we mix the two phases using the CPA and DLM for the spins. Finally, allowing for finite temperatures, we describe the full phase diagram of Ce.

#### A. $f$ -phase shifts and corresponding densities of states

Before presenting our results for the phase diagram, we discuss briefly the scattering properties of a single Ce site. In particular, we concentrate on the phase shifts and corresponding densities of states for  $f$  electrons. In Fig. 1 we show the phase shifts for the SI corrected and uncorrected  $f$  channels of Ce. It can be seen that the uncorrected  $f$  states have a very sharp resonance just above the Fermi energy. The steep resonance corresponds to a long Wigner delay time and indicates that the state is already well localized. The self-interaction corrected  $f$  state is shifted down in energy by about 9 eV, and becomes a bound state (it lies below the muffin-tin zero).

In Fig. 2 we present the density of states and the integrated DOS for the self-interaction corrected  $f$  channel. It can be seen that by integrating Eq. (16) up to the Fermi energy, one collects slightly more than one electron. This is because there is a small density of states in the vicinity of the Fermi level (note the scale of the left-hand-side axis in Fig. 2), which is due to slight hybridization of the SIC channel with the other  $f$  channels whose resonances occur in the vicinity of the Fermi level (see Fig. 1). Some contribution to this density of states might also come from  $5f$  states. This is implied by the behavior of the phase shifts in Fig. 1. The sharp jump by  $\pi$  indicates that the  $4f$  state is a bound state of the SIC potential, and the slow rise of the phase shift above the Fermi energy can be associated with the progression towards the  $5f$  state. Figure 2 also shows that the integrated DOS at the energy where the phase shift goes through  $\pi$ , i.e.,

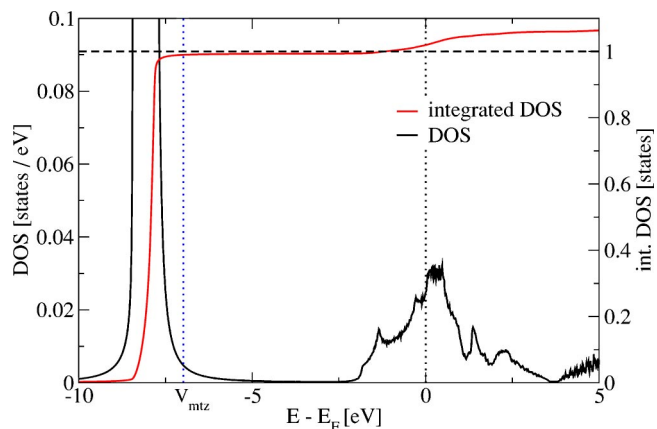


FIG. 2. (Color online) Density of states and integrated density of states of the SI-corrected  $f$  channel.

at about  $-2.5$  eV, is slightly less than 1. This is most likely due to the integration method used to display the quantities in Fig. 2 which is less accurate than the contour integral used in the self-consistent calculations.

#### B. Total energies and equilibrium volumes of Ce $\alpha$ and $\gamma$ phases

In order to determine the ground state configuration of Ce at a given volume, we calculated the total energies for different volumes using the LDA to describe the  $\alpha$  phase and the SIC-LSD formalism for the  $\gamma$  phase, when SI-correcting one localized  $f$  electron, allowed to populate in sequence all possible  $f$  states. In both LDA and SIC-LSD calculations spin-orbit coupling has been neglected for valence electrons, but fully included for core electrons, for which the Dirac equation has been solved. The corresponding total energies as functions of volume are shown in Fig. 3. We find that the LDA, used to represent the  $\alpha$  phase, yields the lowest energy minimum, as seen in Table I. There the ground state properties of the studied configurations are summarized. Table II compares the present results for the ground state configura-

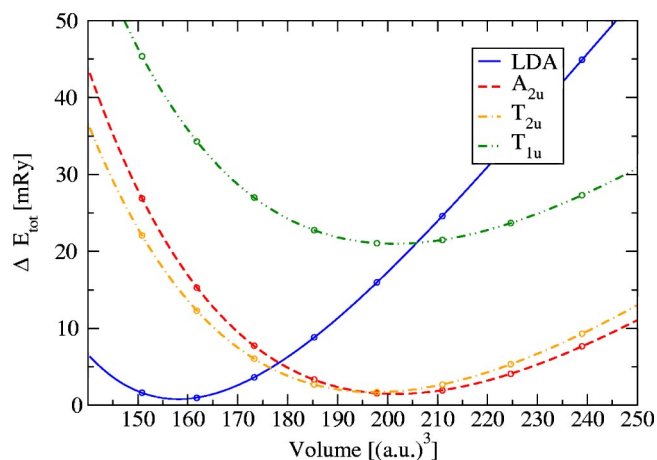


FIG. 3. (Color online) The calculated total energies for Ce from LDA and SIC-LSD, with different  $f$  states localized, as functions of volume, given in atomic units (a.u.)<sup>3</sup>.

TABLE I. The total energy differences as obtained from the LDA and SIC-LSD calculations, with respect to the ground state energy solution (LDA), for Ce in different  $f$  configurations. The corresponding volumes and bulk moduli (evaluated at the theoretical lattice constants) are also given.

		$\Delta E$ (mRy)	$V$ (a.u.) <sup>3</sup>	$B$ (kbar)
LDA		0.0	158	701
	$A_{2u}$	0.8	202	355
SIC	$T_{1u}$	20.3	201	352
	$T_{2u}$	1.5	197	351

tions with previous calculations and with experimental values. Note small differences between the different calculations, which are due to different schemes, and indicate the sensitivity of the results to computational details.

The observed degeneracy of the states within the triplets demonstrates the rotational invariance of the formalism. Note the large crystal field (CF) splitting, separating the  $T_{1u}$  triplet from the other SIC states. As already mentioned, the calculations presented in this section assume a ferromagnetic alignment of the local moments in the  $\gamma$  phase. However, when discussing the phase diagram of Ce, we will also consider the disorder of the local moments using the DLM framework.<sup>23,24</sup>

For the  $\gamma$  phase, treated ferromagnetically, out of the three possible localized states listed in Table I, the state with the  $A_{2u}$  symmetry gives the lowest energy solution. This localized state is also associated with the highest volume among the possible localized configurations. Only 0.8 mRy separate the minima of the  $\alpha$  and  $\gamma$  phases, giving rise to the transition pressure at the absolute zero of about  $-2.3$  kbar. This is in good agreement with the experimental value of  $-7$  kbar,

when extrapolated to zero temperature, and with other theoretical values (see also Table IV). The bulk moduli, given in Table I, are calculated at the theoretical equilibrium volumes. When evaluated at the experimental volumes (as it is common practice in DFT calculations), their values are substantially reduced to 239 kbar for the  $\alpha$  phase and 203 kbar for the  $\gamma$  phase, which is in considerably better agreement with the experimental numbers. The volume collapse (with respect to the volume of the  $\gamma$  phase) is obtained at 22%, which also compares well with the experimental values of 15%–17%. We note that the underestimation of the volumes of both the  $\alpha$  and  $\gamma$  phases is due to the KKR  $l$ -convergence problem, which was addressed by Moghadam *et al.*<sup>34</sup> They demonstrated that angular momenta as high as 16 were needed to obtain satisfactory convergence in the total energy. In the present calculations we choose  $l_{\max}=3$ , which does not seem sufficient for a good description of the equilibrium volumes of the two phases. Although it seems that this  $l$ -convergence problem should affect the LSD and SIC-LSD calculations in a similar manner, we see a significantly larger error for the  $\alpha$  phase, in agreement with the results obtained by other well-known KKR packages when the LDA approximation is implemented to describe the electronic structure of the  $\alpha$  phase.<sup>35</sup> The larger error for the  $\alpha$  phase than for the  $\gamma$  phase (found also in the LMTO-ASA calculations) is most likely due to the fact that LDA is not adequate for describing the experimentally reported correlated nature of the  $\alpha$  phase. In fact, the LDA calculations correspond strictly to the high-pressure  $\alpha'$  phase, which is purely tetravalent and has a smaller lattice constant than the observed  $\alpha$  phase. However, as already mentioned, in our calculations we have treated Ce as a trivalent system (one localized  $f$  electron) in the  $\gamma$  phase, and a tetravalent system (all  $f$  electrons are treated as delocalized) in the  $\alpha$  phase. Experimental data seems to suggest, that  $\alpha$ -Ce has a noninteger valence of 3.67. One could argue

TABLE II. Comparison of the computed equilibrium volumes and bulk moduli with those of other calculations and experiment. The bulk moduli have been calculated at the theoretical equilibrium volumes. Note that unlike in the present, SIC-LSD (KKR) implementation, the results based on the LMTO refer to the full SIC-LSD scheme, involving repeated transformations between real and reciprocal spaces, and Bloch and Wannier representations. The two different sets of LMTO calculations refer to different basis sets and to different ways of solving the SIC-LSD eigenvalue problem. In the reported LDA and GGA calculations the  $\gamma$  phase was modelled by constraining the  $f$  electrons to the core.

Method	$\alpha$ -Ce		$\gamma$ -Ce	
	$V$ (Å <sup>3</sup> )	$B$ (kbar)	$V$ (Å <sup>3</sup> )	$B$ (kbar)
SIC-LSD (KKR) <sup>a</sup>	23.4	701	29.9	355
SIC-LSD (LMTO) <sup>b</sup>	24.7	484	32.6	310
SIC-LSD (LMTO) <sup>c</sup>	25.9	443	34.0	340
LDA <sup>d</sup>	24.5	477	33.7	312
GGA <sup>d</sup>	27.7	391	37.3	288
Expt. <sup>e</sup>	28.2	270	34.7	239

<sup>a</sup>This work.

<sup>b</sup>Reference 31.

<sup>c</sup>Reference 32.

<sup>d</sup>Reference 33.

<sup>e</sup>Taken from Ref. 33.

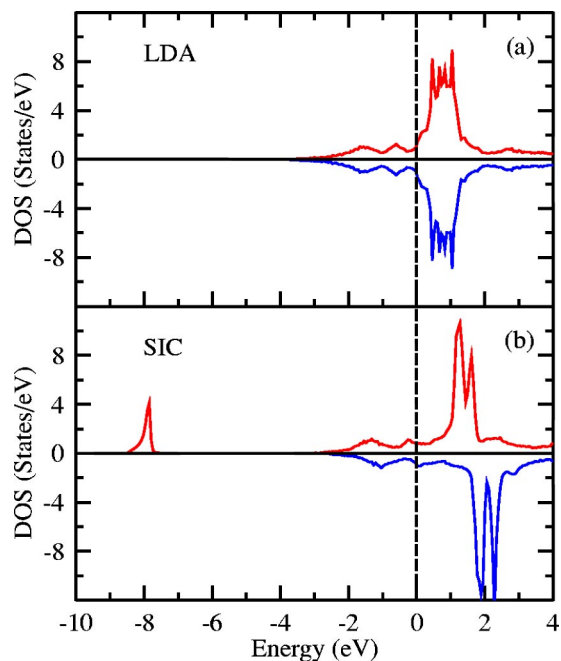


FIG. 4. (Color online) Spin-resolved density of states of Ce in the  $\alpha$  (a) and  $\gamma$  phase (b) with ferromagnetic arrangement of local moments.

that this intermediate valence character of the  $4f$  state could be represented in terms of a pseudoalloy composed of the trivalent and tetravalent Ce atoms. We shall elaborate on this point in one of the following sections.

### C. Densities of states of Ce $\alpha$ and $\gamma$ phases

The densities of states of Ce from the LDA and ferromagnetic SIC-LSD calculations are shown in Fig. 4. The LDA DOS shows all the  $f$  states hybridized into the  $s$ ,  $p$ , and  $d$  states. However, in the SIC-LSD panel of the figure, one clearly sees the split-off localized  $f$  state at about  $-8$  eV. Of course, this does not agree with the spectroscopic position of this state. To accomplish the latter, one would have to take into account the self-energy, which could be evaluated from the total energy difference corresponding to systems with constrained  $f$  occupations.<sup>36</sup> The localized  $f$  state apart, one can clearly see the exchange splitting of the remaining states in the SIC-LSD calculations. The unoccupied  $f$  states in the SIC-LSD density of states are pushed up by 1 eV or so. These unoccupied  $f$  states are furthermore exchange split by 1 eV.

From Table III we note that the number of occupied  $f$

TABLE III. Angular momentum decomposed charges from LDA and SIC-LSD calculations. Note that the  $p$  channel includes the  $5p$  semicore states.

	$s$	$p$	$d$	$f$
LDA	0.40	6.06	2.19	1.35
SIC	0.51	6.16	1.99	1.35

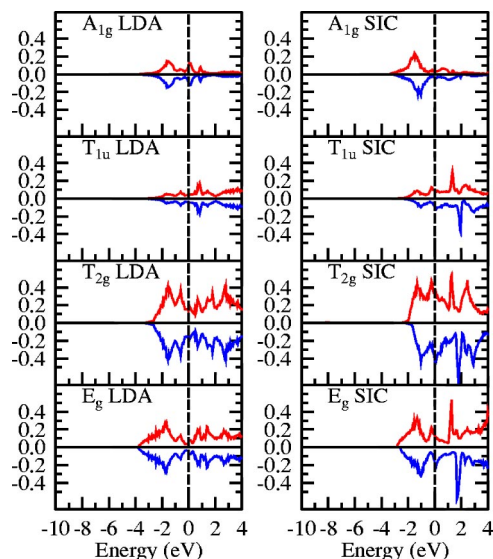


FIG. 5. (Color online) Spin- and symmetry-resolved DOS (in states/eV) for the states originating from  $s(A_{1g})$ ,  $p(T_{1u})$ , and  $d(T_{2g}$  and  $E_g$ ) channels. As in Fig. 4, the SIC-LSD calculation refers to the ferromagnetic arrangement of the local moments.

states hardly differs between the  $\gamma$  phase and the  $\alpha$  phase. This noninteger value of 1.35 in both cases is a consequence of the hybridization of the  $f$  states with the  $s$ ,  $p$ , and  $d$  states seen in Figs. 5 and 6. The number of  $f$  electrons remains constant between the LDA and the SIC-LSD, which might seem rather surprising. What happens is that  $f$  electrons that participate in bonding in the  $\alpha$  phase get transferred to localized electrons in the  $\gamma$  phase. At the same time some of the bonding  $d$  electrons are transferred to the repulsive  $sp$  channel. These effects conspire to give the larger lattice constant for the  $\gamma$  phase.

The  $s$ ,  $p$ , and  $d$  spin-resolved densities of states of Fig. 5 show remarkably rigid band behavior between the LDA and SIC with the Fermi energy moving down with respect to the

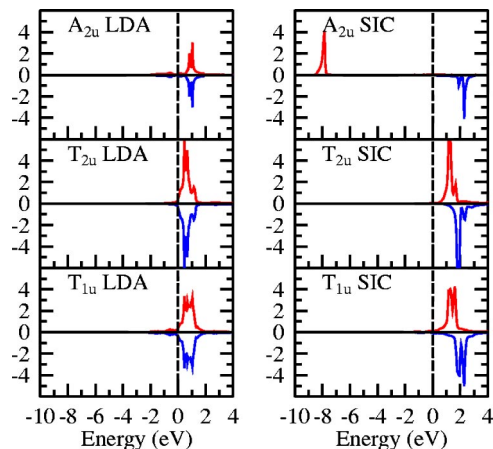


FIG. 6. (Color online) Spin- and symmetry-resolved DOS (in states/eV) for the states originating from  $f$  channels. Note the different scale of the plot with respect to Fig. 5. As in Fig. 4, the SIC-LSD calculation refers to the ferromagnetic arrangement of the local moments.

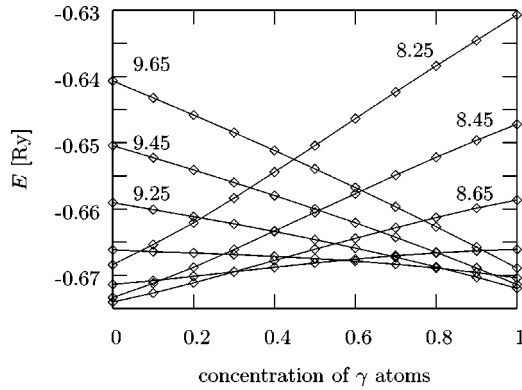


FIG. 7. Total energies ( $T=0$  K) of the Ce  $\alpha$ - $\gamma$  pseudoalloy as a function of the concentration of localized states. The curves correspond to the lattice constants, indicated in the figure. The labels of 8.85 and 9.05, corresponding to the remaining curves, have been omitted for readability.

SIC-LSD  $d$  partial density of states. We also note that in Fig. 6 the unoccupied  $f$  states are well separated from the Fermi level, because the Fermi energy is lowered, and the hybridization with the occupied  $s$ ,  $p$ , and  $d$  states has been substantially reduced. These changes in the  $s$ ,  $p$ , and  $d$  densities of states are also reflected in Table III where we see a reduction of 0.2 electrons in the  $d$  channel of the localized phase and a corresponding increase of 0.1 electrons in both the  $s$  and  $p$  channels of the localized phase. Even though the Fermi energy moves down in the localized phase, we see from Fig. 5 that the number of occupied states in the  $s$  and  $p$  channels has increased.

#### D. Ce $\alpha$ - $\gamma$ pseudoalloy

In order to improve on the LDA representation of correlations in the  $\alpha$  phase of Ce, in the present approach, in the spirit of the Hubbard III approximation,<sup>19</sup> one can model the experimentally implied noninteger valence of the Ce ions by a pseudoalloy consisting of the trivalent (SIC-LSD) Ce ions with concentration  $c$ , and the tetravalent (LDA) Ce ions with the concentration  $(1-c)$ . In addition, taking into account the disordered local moments of the trivalent Ce ions in the  $\gamma$  phase, one can assume that their up and down orientations occur with equal probabilities. Supposing homogeneous randomness, such a ternary pseudoalloy can be described by the coherent potential approximation (CPA). The respective concentrations of the trivalent and tetravalent Ce ions in the pseudoalloy are then determined by minimizing the total energy for each volume with respect to the concentration  $c$ .

In Fig. 7 we show the total energies for the  $\alpha$ - $\gamma$  pseudoalloy at  $T=0$  K, in which the  $\gamma$  phase occurs with the concentration  $c$  ( $c/2$  for each spin orientation), and the  $\alpha$  phase with the concentration  $(1-c)$ , for several lattice constants. It can be seen that all shown total energy curves have their minima either at  $c=0$  (pure  $\alpha$  phase) or  $c=1$  (pure  $\gamma$  phase). Hence a fractional occupation of the  $4f$  state appears to be energetically unfavorable for all lattice constants. From these calculations we can conclude that a static, single-site approximation is not sufficient to describe the intermediate valence

state of  $\alpha$ -Ce at  $T=0$  K. These calculations are consistent with the earlier results by Svane who performed supercell calculations to model 25%, 50%, and 75% of  $\alpha$ - $\gamma$  admixtures, but treating the  $\gamma$  phase ferromagnetically and not as a DLM phase.<sup>32</sup> There too, no total energy minimum was found for intermediate concentrations between 0 and 1, and also a mainly convex (from above) curvature for the total energy, as a function of concentration, was obtained. This suggests that to describe the intermediate valence state of the  $\alpha$  phase one would need to consider a dynamical generalization of the CPA,<sup>26</sup> which would involve dynamical fluctuations between the trivalent and tetravalent states. Other possible mechanisms to favor intermediate valence will be commented about in Sec. VIII.

#### E. Ce $\alpha$ - $\gamma$ spectral functions

In this section we discuss the spectral functions along the  $\Gamma$ - $X$  line, calculated for the pseudoalloy consisting of 50%  $\gamma$ -admixture into the  $\alpha$  phase, i.e., 50%  $\alpha$ , 25%  $\gamma$  spin-up and 25%  $\gamma$  spin-down, in comparison with the spectral functions of the pure phases, all at the same volume, as shown in Fig. 8. The pure  $\gamma$  phase has been represented by a 50% spin-up and 50% spin-down alloy. The pure  $\alpha$  phase [panel (a)] shows a well-defined band structure. (The minor smearing of the bands is due to a small imaginary part added to the energy.) Of course, the LDA leads trivially to a non-spin-polarized band structure, but the absence of an exchange splitting in panels (b) and (c) is due to the use of DLM, which defines an effective medium in which the local moments are averaged out. In the panels (b) and (c) the broadening of the spectral functions is apparent. The actual linewidth of the spectral function can clearly be seen in Fig. 9, showing the spectral functions at the  $\Gamma$  point. Here, similarly to the smearing effect seen in Fig. 8, the residual linewidth seen in panel (a) is purely due to the small imaginary part of the energy, necessary to obtain well behaved  $\tau$  matrices.

The spectral functions reveal some features of the current approach. First, it can be seen that the  $s$ - and  $d$ -derived states at the  $\Gamma$  point are hardly affected by the CPA. These states have no hybridization with the SI-corrected  $f$  state. Symmetry analysis of the spectral function, shown in panel (b) of Fig. 9, reveals that the  $A_{2u}f$  state appears twice (the peak at  $-8$  eV and the sharp shoulder just above the Fermi energy), since we are in the split-band regime. Due to the DLM treatment of the  $\gamma$  phase, this feature is also seen in panel (c), where the upper of the split-band peaks merges with the lower triplet  $f$  peak. The two triplets ( $T_{1u}$  and  $T_{2u}$ ) show common band behavior. The corresponding broadenings are very different between panels (b) and (c). Moreover, panel (c), as compared to panel (a), also shows that the unoccupied  $f$  states have been pushed up in energy, because the localized  $f$  electron is more effective in screening the nuclear charge. This results in an energy splitting of the  $\alpha$  and  $\gamma$  unoccupied triplets which leads to a broadening of the unoccupied triplets, as seen in panel (b). The shoulder at about 1 eV is an indication that the splitting is noticeable on the scale of the dispersion of the bands. The broadening of the triplets is reduced in panel (c) where no  $\alpha$  phase is admixed and where

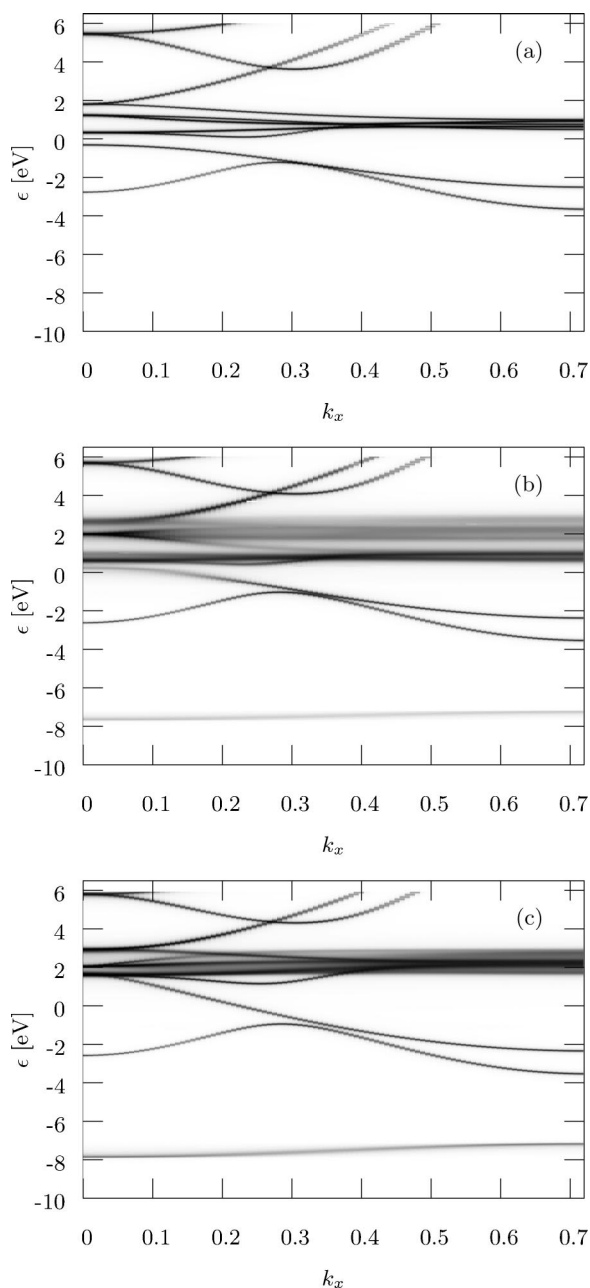


FIG. 8. Spectral functions along  $\Gamma$ -X, relative to the Fermi level, for the  $\gamma$ -phase concentration 0 in panel (a), 0.5 in (b), and 1 in (c), respectively. The spectral functions were calculated at the lattice constant  $a=8.65$  a.u.

the broadening of the lower triplet state is a consequence of merging with the upper split-band peak of the singlet state. Note that the  $f$  states at the Fermi level have a finite lifetime which might indicate a shortcoming of the static CPA for the description of an intermediate valence, a coherent mixture of the localized and delocalized states in terms of wave functions might be a more appropriate description.

#### F. Phase diagram

In this section we concentrate on the finite temperature phase diagram of Ce. The idea of describing Ce at finite

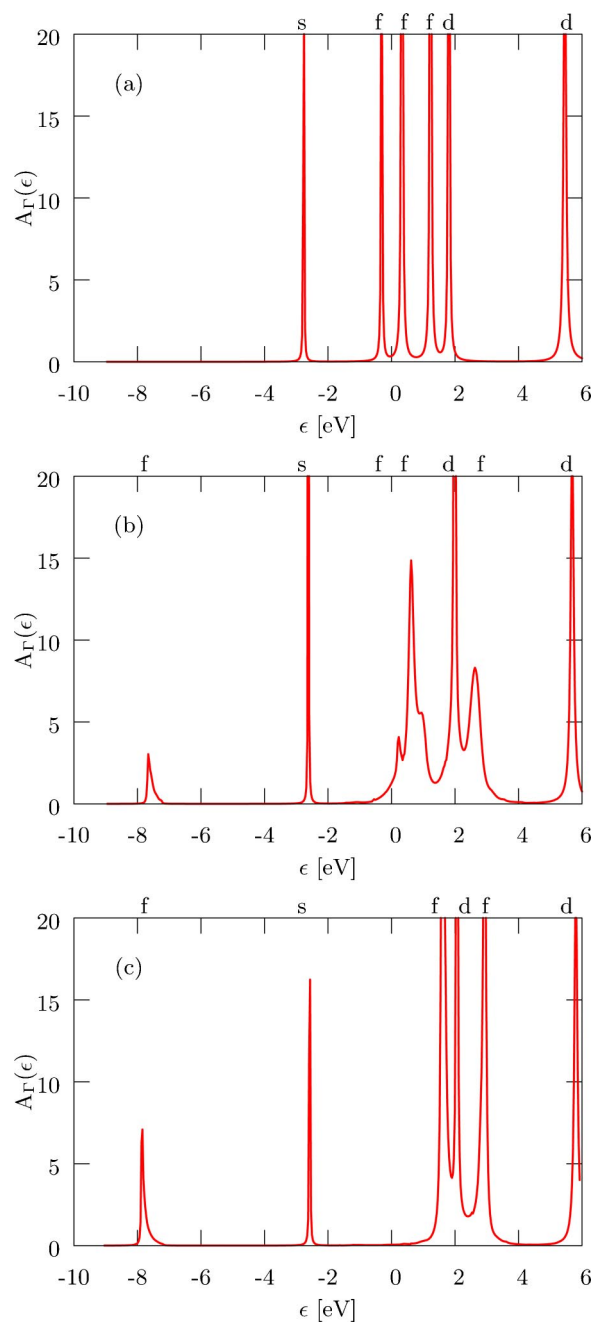


FIG. 9. (Color online) Spectral functions at the  $\Gamma$  point for the  $\gamma$ -phase concentrations 0 (a), 0.5 (b), and 1 (c). The character of the respective peaks is marked above the upper horizontal line of each panel.

temperatures as a pseudoalloy of  $\alpha$ - and  $\gamma$ -Ce atoms was first put forward by Johansson *et al.*<sup>33</sup> and by Svane.<sup>32</sup> Since at finite temperatures the thermal (classical) fluctuations are of major importance, the static approximation should suffice. In the work by Johansson *et al.* the pseudoalloy was treated by the CPA implemented within the LMTO method, where the  $\gamma$  phase was modeled by including the  $4f$  states into the core, while in the  $\alpha$  phase the  $f$  states were treated as band states. Due to the different treatment of both phases, their total energies could not be compared and the energies of the  $\gamma$  phase had to be adjusted by hand to yield the correct  $\alpha$ - $\gamma$  transition

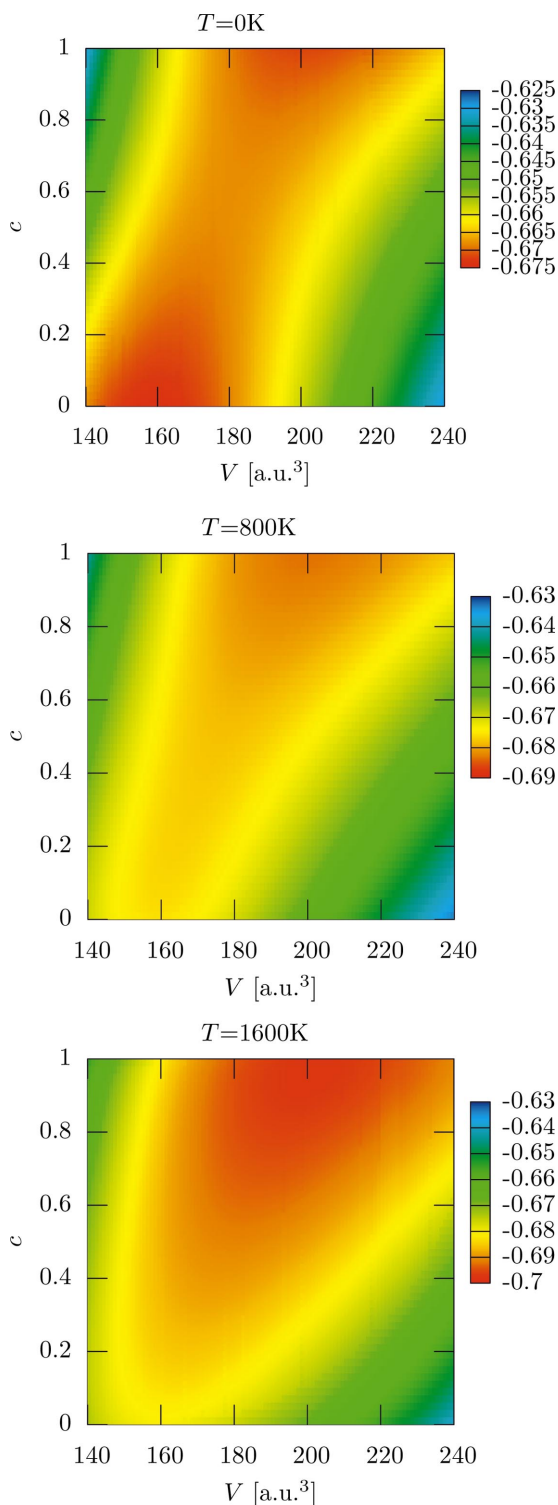


FIG. 10. (Color) Calculated free energies for the temperatures  $T=0, 800,$  and  $1600$  K. The plots represent fits to the calculations, which have been performed for concentrations from 0 (corresponding to the pure  $\alpha$  phase) to 1 (corresponding to the pure  $\gamma$  phase), in steps of 0.1, and for lattice constants from 8.25 a.u. to 9.65 a.u., in steps of 0.2 a.u. A constant of 17 717 Ry has been added to all energies.

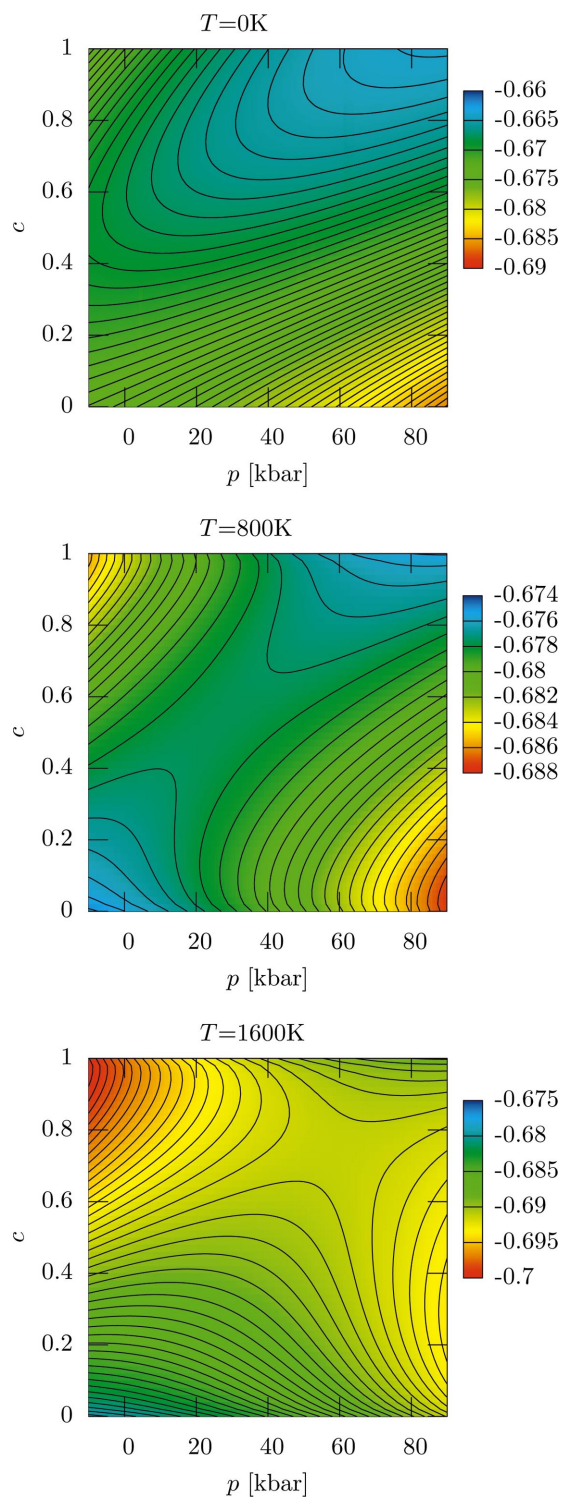


FIG. 11. (Color) Gibbs free energies for  $T=0, 800,$  and  $1600$  K. In order to enhance the readability of the plots the energies have been calibrated by a linear term, proportional to pressure.

pressure at zero temperature. Svane, on the other hand, described the  $\gamma$  phase as a ferromagnet using the LMTO-SIC, thus treating both phases on equal footing, and utilizing a supercell to mimic the pseudoalloy at only a few accessible concentrations. From these calculations he concluded that a

linear interpolation of the  $\alpha$  and  $\gamma$  energies to arbitrary concentrations should be adequate enough.

Here we present calculations which combine both the CPA and the SIC-LSD to describe the  $\gamma$  phase as a DLM system, treated as a ternary alloy, consisting of spin-up and spin-down SIC sites with concentrations  $c/2$  each, and LDA sites with the concentration  $(1-c)$ . In addition, we go beyond the scope of previous works by taking into account the effect of finite temperatures on the electronic total energies and the electronic contribution to the entropy, as defined in Sec. VI. However, the vibrational entropy,  $S_{\text{vib}}$ , is neglected in the presented results. We shall briefly comment on its effect on the calculated phase diagram in the next section where we analyze in detail how different aspects of the present calculations influence the final results.

Ideally, one would like to treat a pseudoalloy, which consists of all possible states of a Ce ion, i.e., the LDA, and all possible SI-corrected  $f$  states. This would give rise to a pseudoalloy consisting of 15 components, the LDA plus the 14 possible  $f$ -SIC states (including the spin multiplicity). Since this would be quite a formidable task, we use a simplified approach. Figure 3 indicates that crystal-field splitting gives rise to nearly degenerate  $A_{2u}$  (singlet) and  $T_{2u}$  (triplet) states, while the  $T_{1u}$  triplet lies 20 mRy higher in energy. At the temperatures considered here, the  $T_{1u}$  states are thermally not accessible. Thus treating the remaining eight states as degenerate, leaves us with a nine component pseudoalloy, with the constraint that the concentrations of the considered eight SIC states are equal and can be set to  $c/8$ . It is easy to show that in this case, in addition to the mixing entropy defined in Sec. VI one has to take into account a term

$$S_{\text{mag}}(c) = k_B c \ln 8, \quad (26)$$

arising from this eightfold multiplicity. Note that in previous studies, where the CF splitting has not been taken into account, the magnetic entropy was assumed to be that of a spin-orbit (SO) coupled  $J=5/2$  state, i.e.,  $S_{\text{mag}}(c) = k_B c \ln 6$ . In the next section we shall comment on how the two different magnetic entropy terms influence the critical characteristics of the calculated phase diagram.

We performed calculations for several lattice constants, embracing the equilibrium lattice constants of both phases, and concentrations from 0 to 1, in steps of 0.1. The results for the free energies of the three selected temperatures are shown in Fig. 10. In the  $T=0$  K panel one clearly sees the two minima, corresponding to the pure  $\alpha$ -phase (LDA) and the pure  $\gamma$ -phase (SIC-LSD) calculations. The equilibrium lattice constant for a given concentration  $c$  interpolates between the two extremes, and it is apparent that an intermediate valence state, even if not energetically favorable, would correct the underestimated lattice constant of the  $\alpha$  phase. As the temperature is increased, the free energy surface gets strongly tilted towards the SIC-LSD side and now shows only one broad minimum. This is mainly due to the magnetic entropy.

Although the concentration-dependent free energies are the quantities directly accessible from the calculations, they do not easily reveal the full information on the phase dia-

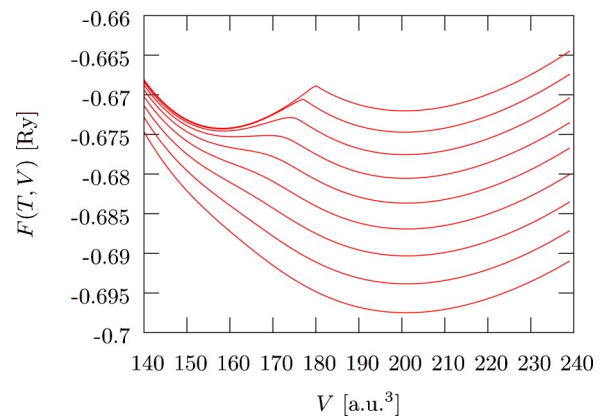


FIG. 12. (Color online) The free energies as function of the volume for the temperatures 0 (highest curve), 200, 400, 600, 800, 1000, 1200, 1400, and 1600 K (lowest curve). A constant of 17 717 Ry has been added to all energies.

gram. In order to determine the full  $p$ - $T$  phase diagram, it is necessary to calculate the Gibbs free energy,

$$G(T, c, p) = F(T, c, V(T, c, p)) + pV(T, c, p). \quad (27)$$

The Gibbs free energies are displayed in Fig. 11. From them, at each given pressure and temperature, we can determine the concentration of the trivalent Ce, by minimizing the Gibbs free energy with respect to  $c$ . At zero temperature one finds (for low pressures) two local minima, associated with  $c=0$  and  $c=1$ . By increasing the pressure, the order of the minima changes and the minimizing concentration jumps from 1 to 0. At higher temperatures the minima start moving towards intermediate concentrations. Only above the critical temperature, one finds the minimum smoothly changing from low to high concentrations.

We can obtain the free energy of the physical system at a given volume by evaluating the concentration dependent free energy at the minimizing concentration  $c_{\text{min}}$ ,

$$F(T, V) = F(T, c_{\text{min}}, V). \quad (28)$$

These free energies are displayed in Fig. 12, which clearly shows the double-well behavior for low temperatures, which is gradually smoothed out with increasing temperatures. Furthermore one finds that, at elevated temperatures, the free energy is mainly lowered at large lattice constants, corresponding to the  $\gamma$  phase, with its larger entropy.

Inserting the minimizing concentration  $c_{\text{min}}$  into the pressure-volume relation

$$p(T, V) = p(T, c_{\text{min}}, V) = - \frac{\partial}{\partial V} F(T, c_{\text{min}}, V) \quad (29)$$

allows to calculate the isotherms of Ce, which are displayed in Fig. 13. It can be seen that the average valence, close to the coexistence line, gradually changes with increasing temperature. Above the critical temperature, the valence changes continuously with increasing pressure from trivalent to tetravalent.

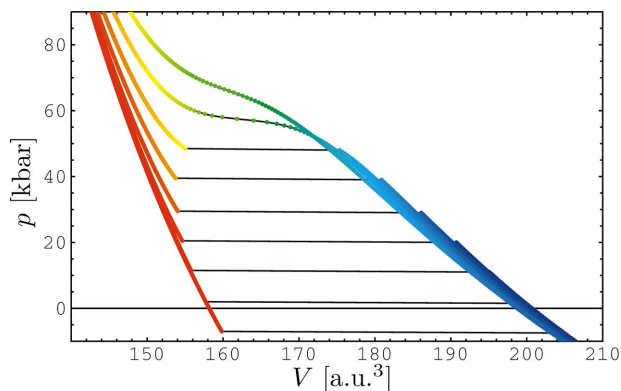


FIG. 13. (Color) Calculated isotherms for the temperatures  $T=0$  (lowest curve), 200, 400, 600, 800, 1000, 1200, 1400, and 1600 K (highest curve). The color indicates the fraction of localized electrons, blue is all localized ( $\gamma$  phase), and red is all delocalized ( $\alpha$  phase).

In Fig. 14 we present phase diagram, obtained from the free energies of the  $\alpha$ - $\gamma$  pseudoalloy, with the  $\gamma$  phase described by the DLM approach. It can clearly be seen in the figure how the transition becomes continuous above the critical temperature. The experimentally observed critical point (600 K, 20 kbar) falls on top of the calculated phase separation line, which starts at the zero temperature transition pressure of  $-7.4$  kbar. This means that the slope of the phase separation line is in very good agreement with experiments. The critical temperature overestimates the experimental one by roughly a factor of 2, which is still reasonable considering that the critical temperature is very sensitive to various small details of the calculations and in particular the theoretical lattice parameters of both the Ce phases. Note that the  $T_c$  at zero pressure of 169 K (see Table IV) compares well with the experimental value of  $141 \pm 10$  K.

Finally we examine in more detail the discontinuity across the phase separation line. Figure 15 shows the magnitude of

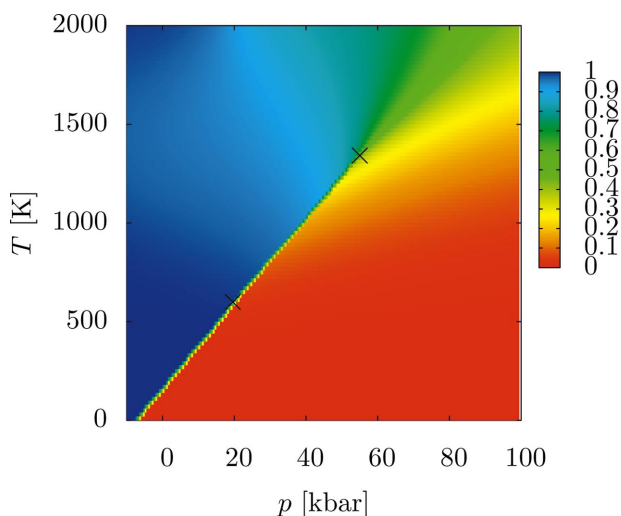


FIG. 14. (Color) Phase diagram obtained for the pseudoalloy, composed of  $\alpha$ - and  $\gamma$ -Ce. The crosses indicate the calculated and experimental critical points. The color indicates the fraction of localized electrons, blue is all localized ( $\gamma$  phase), and red is all delocalized ( $\alpha$  phase).

the discontinuities for the various ingredients of the Gibbs free energy. As expected, all contributions vanish at the critical temperature, above which there is a continuous crossover between the  $\alpha$  and the  $\gamma$  phase. It also can be seen from this figure that the entropy discontinuity is by far the largest contribution. The phase transition is therefore driven by entropy, rather than by energetics. The entropy discontinuity itself is mainly determined by the magnetic entropy.

### G. Analysis of results

In order to investigate the importance of the different aspects of the present calculations (i.e., the DLM description of the  $\gamma$  phase, the inclusion of finite temperature effects in the electronic free energy, and the CPA itself), as compared to earlier studies, we have also performed a set of calculations where, selectively, we neglect some of these effects and look at the consequences. In particular, we study the influence of these effects on the critical temperature and the slope of the phase separation line. The results of these calculations are summarized in Table IV, in comparison with the results of earlier theoretical, as well as, experimental studies.

First we focus on the importance of the disordered local moments representation of the  $\gamma$  phase. By comparing the DLM results in Table IV with those marked by Ferro (ferromagnetic calculations for the  $\gamma$  phase), one finds that the DLM calculations lead to a moderate lowering of the critical temperature, and a more negative zero temperature transition pressure. This can easily be understood, since at zero temperature, the ferromagnetically ordered phase has a lower energy as compared to the disordered phase. Experimentally such a magnetic order is not observed, since at low temperatures (and positive pressures) Ce is in its nonmagnetic  $\alpha$  phase. The lowering of the critical temperature cannot be easily identified with a specific aspect of the DLM calculations, since many effects, such as the curvature of the free energies with respect to the concentration, but also the anharmonic terms in the total energy as a function of volume, conspire to determine the phase diagram.

The second point is the effect of finite temperature on the total energy and the electronic entropy. In earlier studies of the phase diagram,<sup>32,33,40</sup> the electronic structure calculations were performed at zero temperature, and the finite temperature effect entered only via the mixing entropy, the magnetic entropy and in Ref. 33 also the vibrational entropy. This means that  $E_{\text{tot}}(T, c, V)$  was replaced by  $E_{\text{tot}}(0, c, V)$  and the electronic entropy  $S_{\text{el}}$  was neglected. In Fig. 16, we analyze the difference between the electronic free energy  $F_{\text{el}}(T, c, V) = E_{\text{tot}}(T, c, V) - TS_{\text{el}}(T, c, V)$  and the total energy at  $T=0$ . The difference  $F_{\text{el}}(T, c, V) - F_{\text{el}}(0, c, V)$  exhibits a moderate dependence on the concentration. The larger effect for the  $\alpha$  phase is easily explained using a low temperature expansion. The main effect of the finite temperatures is the broadening of the Fermi function. To lowest order in temperature, the change of the free energy is proportional to the density of states at the Fermi level. The effect on the phase diagram can be seen in Table IV by comparing the columns I and II. Neglecting these finite temperature effects gives rise to an increase of the critical temperature by roughly 200 K,

TABLE IV. The critical temperature and pressure, as well as, the zero temperature and room temperature transition pressures and the zero pressure transition temperature for different calculations: DLM and Ferro refer to the disordered or ferromagnetic alignment of the local moments in the  $\gamma$  phase, CF and SO indicate the crystal field or spin-orbit scenario, as discussed in the text. The index I denotes calculations with finite temperature effects included in the band structure and the CPA, II refers to the neglect of these finite temperature effects, and III represents calculations, where in addition the concentration dependence was approximated by a linear interpolation. The main results, which are also shown in the figures, are the DLM-CF (I) calculations, printed as bold in the table.

	DLM-CF			DLM-SO			Ferro-CF			Ferro-SO			Svane <sup>a</sup>	Johansson <sup>b</sup>	KVC <sup>c</sup>	Prom <sup>d</sup>	Expt.
	I	II	III	I	II	III	I	II	III	I	II	III					
$T_c$	<b>1377</b>	1528	1129	1407	1568	1157	1444	1660	1139	1471	1689	1166	1300	980	520	600	600
$p(T_c)$	<b>56</b>	62	51	47	52	43	64	74	58	53	61	49	47	39	39	18	20
$p(T=0\text{ K})$	<b>-7.4</b>	-7.4	-7.4	-7.4	-7.4	-7.4	-2.3	-2.3	-2.3	-2.2	-2.3	-2.3	-1.0	-6	-6		-7
$p(T=300\text{ K})$	<b>6.1</b>	6.2	6.2	4.1	4.2	4.2	11.0	11.4	11.4	9.0	9.5	9.5	10	7	8	6	6
$T_c(p=0)$	<b>169</b>	167	167	196	194	194	52	52	52	61	61	61		135			140±10

<sup>a</sup>Reference 32.

<sup>b</sup>Reference 33.

<sup>c</sup>Kondo volume collapse model, Ref. 38.

<sup>d</sup>Promotion model, Ref. 39.

while the slope of the phase separation line remains unaltered.

Next is the effect of the CPA. In the study by Svane,<sup>32</sup> it was suggested that the weak departure from linearity of the total energy curves as a function of concentration (Fig. 7) did not play an important role. Thus, we recalculated the phase diagram, replacing the full concentration dependence of the total energy by the linear interpolation

$$E_{\text{lin}}(c, V) = (1 - c)E(0, V) + cE(1, V). \quad (30)$$

The effect of this approximation can be seen in Table IV by comparing the columns II and III, respectively. Both sets of calculations use the  $T=0\text{ K}$  total energies only. The transition temperature obtained from the linear interpolation is strikingly reduced, in comparison to the CPA calculation, and similar to the one reported by Svane. As pointed out by Jo-

hansson *et al.*,<sup>33</sup> the critical temperature is to a large extent determined by the mixing entropy. Without the mixing entropy one would at all temperatures find a sudden transition (with a finite volume collapse) between the low- and high-pressure phases. The mixing entropy will, if the temperature is high enough, lead to a minimum of the free energy for an intermediate concentration of the  $\gamma$  phase, eventually resulting in a continuous crossover between the low-pressure and the high-pressure phases. As seen in Fig. 7, the CPA gives rise to a convex (from above) curvature of the total energies. It effectively reduces the mixing entropy and increases the critical temperature. It can also be seen that within this linear approximation, the difference between the DLM and the Ferro calculations is strongly reduced, which means that the main effect of DLM is not only the energy lowering of the  $\gamma$  phase, but more importantly a different shape of the energy versus concentration curves.

Last, we discuss the effect of the degeneracy of the  $\gamma$  phase ground state. As described above, in the CF calculations a degeneracy of 8 was used, corresponding to almost degenerate  $A_{2u}$  and  $T_{2u}$  states, arising from a crystal field

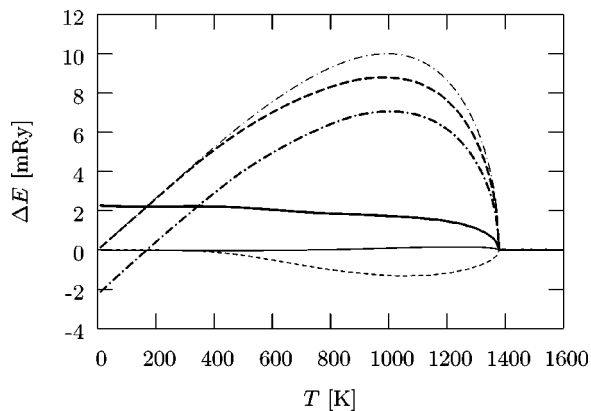


FIG. 15. Discontinuities of the total energy (thick solid line), the total entropy  $TS$  (thick dashed line), and the  $pV$  term (thick dashed-dotted line) over the phase separation line as function of the temperature. The entropy term is further decomposed into the electronic (thin solid line), the mixing (thin dashed line), and the magnetic (thin dashed-dotted line) contribution.

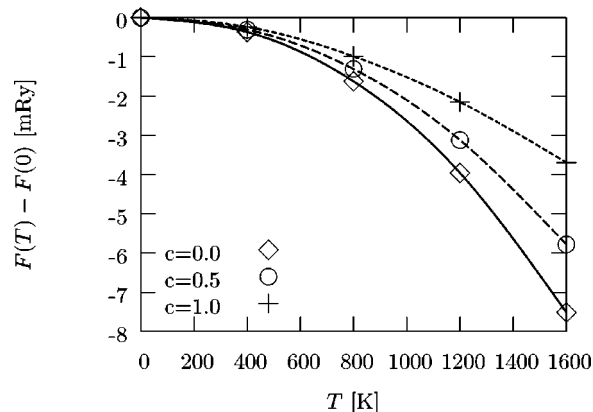


FIG. 16. Temperature dependence of the electronic free energy, as defined in the text.

splitting. The results to be compared here are shown in the columns CF and SO of Table IV. In the SO scenario, the term proportional to  $\ln 6$ , corresponding to a  $J=5/2$  state, was used for the magnetic entropy, instead of  $\ln 8$ , as in the CF scenario. One can see that the magnetic entropy, being linear in  $c$ , determines mostly the slope of the phase separation line and has only a minor effect on the magnitude of the critical temperature. The results obtained with the DLM and the magnetic entropy due to the CF splitting show better agreement of the calculated transition pressures with experiment. This, however, may be due to a cancellation of errors. The slope of the phase separation line is mainly given by the ratio  $(S_\gamma - S_\alpha)/(V_\gamma - V_\alpha)$ , where  $S_{\alpha(\gamma)}$  and  $V_{\alpha(\gamma)}$  are the  $T=0$  values of the entropy and the volume of the  $\alpha(\gamma)$  phase.

Due to the larger underestimation of the volume of the  $\alpha$  phase, the volume collapse is slightly overestimated in our approach. Therefore the higher value of the entropy difference in the CF scenario, as opposed to the SO scenario, leads to a better agreement with the experimental slope. It should be noted though that these calculations do not include the vibrational entropy. To estimate the effect of this vibrational entropy, we recalculate the phase diagram using a simple model for the vibrational entropy, namely

$$S_{\text{vib}}(c) = -k_B c \Delta S_{\text{vib}}^{\gamma-\alpha}, \quad (31)$$

with the value of  $\Delta S_{\text{vib}}^{\gamma-\alpha} \approx 0.75$ , as suggested by Jeong *et al.*<sup>41</sup> In doing so, the critical temperature is only slightly reduced to 1292 K, while the critical pressure increases to 69 kbar. In view of the above discussion, it is not surprising that a contribution, which is purely linear in  $c$ , basically affects only the critical pressure. We conclude from this result that this simplified model for the vibrational entropy is too crude and a more sophisticated one should be put in place. One should add here that Johansson *et al.*<sup>33</sup> have employed a Debye-Grüneisen model, while Svane<sup>32</sup> has completely neglected the vibrational entropy.

Finally, we would like to comment on the finding of Nilsson *et al.*<sup>42</sup> that the disordered local moments can give rise to a localization of  $f$ -electrons. From our DLM only calculation, without applying SIC, we found that it is not possible to stabilize a local moment in Ce, except at very large volumes, where even the LSD yields a magnetic solution.

### VIII. DISCUSSION

As already mentioned, experiments indicate that the  $\alpha$  phase is not composed of tetravalent Ce atoms, but is rather described by an intermediate valence of 3.67.<sup>30</sup> From Fig. 10, we see that an intermediate valence, i.e., a fractional concentration ( $0 < c < 1$ ), would lead to an increased equilibrium lattice constant. One can simulate the effect of the intermediate valence for the  $\alpha$  phase by simply rescaling the concentrations when evaluating the phase diagram. In Fig. 17 we present the critical points of the phase transition obtained when we represent the  $\alpha$  phase by a nonzero concentration,  $c_0$ , of the trivalent Ce atoms, added into the host of tetravalent Ce atoms. As can be seen in the figure, the critical temperature quickly decreases with the increase of the ad-

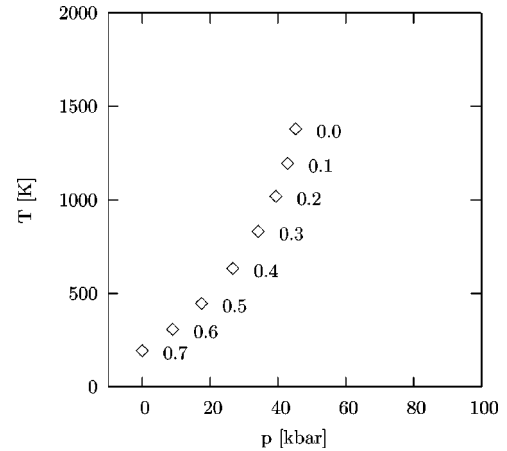


FIG. 17. Critical points of the phase transition, obtained when the concentration of trivalent Ce atoms in the  $\alpha$  phase is artificially fixed at a finite  $c_0$ . The points are marked by their corresponding value of  $c_0$ , where  $c_0=0$  represents purely tetravalent Ce.

mixture of trivalent Ce in the  $\alpha$  phase. In this calculation, the SIC-LSD energies have been uniformly calibrated to keep the zero temperature transition pressure at its original value of  $-7.4$  kbar. It can be seen in the figure that the best value for critical temperature is obtained for  $c_0 \approx 0.4$ , which corresponds to an intermediate valence of 3.6.

The intermediate valence scenario for the  $\alpha$  phase, as discussed above, could result from dynamical fluctuations. These fluctuations could be realized by describing Ce as a two level system (TLS). We will elaborate on this idea in Sec. IX. A mechanism, based on the dynamical interaction of two states will, quite generally, be more effective if the two states are close in energy. Looking at the total energy as a function of the lattice spacing and the concentration (Fig. 10), one finds that the pure  $\alpha$  and  $\gamma$  solutions (LDA and SIC-LSD, respectively) are degenerate close to  $a=8.9$  atomic units. The interaction of these two states will lower the total energy at these lattice constants, and eventually might establish them as the global minimum. The increased lattice constant would be closer to experimental values. Clearly such a state would be neither described by full localization nor delocalization of the  $f$  electron, but would be better characterized as an intermediate valence state. In the following section we will outline how we envision this two-level system to work.

The next point we want to discuss is the effect of lattice relaxations. In the intermediate valence regime (as described by the static CPA) there is a rather large size mismatch between the  $\alpha$  and the  $\gamma$  atoms, which may give rise to strong internal strains. Allowing for lattice relaxations, which are not considered here, would give rise to an energy lowering for intermediate concentrations and could lead to intermediate valence, even in the static limit, and hence to the reduction of the critical temperature.

Another factor that might have a significant influence on the phase diagram and its characteristics is associated with the single-site aspect of the CPA. Being a single-site theory, the CPA cannot deal with order in disorder, namely with short range order (SRO) in the distribution of the alloy con-

figurations. However, even in the disordered phase it must be important to distinguish situations where the nearest neighbors are preferentially like atoms from those where they are unlike atoms. Such short range order is expected to lower the free energy of the disordered state and hence lower  $T_c$  of the  $\alpha$ - $\gamma$  phase transition. In addition, it should influence the energetically favorable relative concentration of the two different components of the alloy. Thus by taking SRO into account one might be able to move beyond the primitive alloy analogy and improve on the present LSIC-KKR-CPA approach. The way it could be accomplished is by implementing the nonlocal extension of the KKR-CPA,<sup>45-47</sup> which would allow to treat possible correlated valence fluctuations near the  $\alpha$ - $\gamma$  phase transition in Ce.

Finally, the phase diagram of Ce suggests that at negative pressure there could exist a quantum critical point (QCP), i.e., a localization-delocalization transition at zero temperature, driven by pressure. The vicinity of this QCP, although it is not accessible experimentally, could still influence the physics of the material in the accessible positive pressure range. The quantum fluctuations, which are responsible for the transition, should also be visible in its vicinity and could explain the correlated nature of the  $\alpha$  phase.

## IX. OUTLOOK

Several times in this article we have referred to the possibility of going beyond the theory outlined above by allowing for dynamical valence and spin fluctuations. In short, the suggestion is that, as above, we regard the self-interaction corrected and the not so corrected version of the local potential at a site, as corresponding to two states of the atom and allow for such atom to tunnel between the two states  $|a\rangle$  and  $|b\rangle$ , which would form a two-level system. Electrons interacting with such TLS were already thoroughly studied in the context of metallic glasses.<sup>43</sup> In the present scenario such a procedure would address the valence fluctuations. On the other hand, identifying the possible spin states of the SI-corrected system with the two levels<sup>51</sup> would constitute a possible dynamical generalization of the DLM formalism, taking into account dynamical spin fluctuations. This might describe the Kondo screening of the local moments at low temperatures.

Many of the consequences of such interactions are by now well known.<sup>44</sup> In such studies the TLS is an atom tunneling between two nearly degenerate positions in a metallic environment.<sup>44</sup> The physics is particularly interesting in the case of assisted tunneling where the TLS changes its state as an electron scatters from it. However, it should be stressed that in the cases where the atom changes its position in the tunneling process, the TLS is external to the electron system while in the proposed model it is designed to capture the physics of a slowly changing collective degree of freedom of the electrons themselves. In this sense our TLS is very much like the DLM in paramagnetic metals.

From the point of view of the present perspective the most directly relevant work on external TLS's is that of Vldar *et al.*<sup>48</sup> They show that, if the TLS couples two or more angular momentum states, as the temperature is lowered the high

temperature pseudoalloy phase gives way, at a characteristic temperature  $T_K$  to a ground state which is an orbital analogue of Kondo singlets of magnetic impurities in metals. In the case of the LDA/SIC-LSD TLS, this means, that at high temperatures, we would find the pseudoalloy, as described above, while at low temperatures, the system would be neither in the LDA, nor in the SIC-LSD state, but would be in an intermediate valence ground state. Clearly, such dynamical fluctuations may also help to reduce the critical temperature if the generalized Kondo temperature, associated with the TLS, is not too small.

As a final remark concerning the dynamical generalization of our disordered local valence calculations we note that the above model is an analogue of Yuval and Anderson's Kondo Hamiltonian approach to the magnetic impurity problem, as opposed to the full dynamical calculation based on the Anderson model, deployed for the same problem by Hamann.<sup>49,50</sup> The relevant point to stress is that these two calculations yield, in the appropriately asymptotic, namely scaling, regime the same results. Thus, they lend credit to the above proposed short-cut to a first principles DMFT treatment of our fluctuating valence problem.

## X. CONCLUSIONS

We have presented a multiple scattering, implementation of the SIC-LSD formalism for solids within KKR band structure method, combined with the CPA description of intermediate valences. The method has been illustrated on the application to the Ce  $\alpha$ - $\gamma$  phase transition. The results have been discussed in detail, highlighting the functionality and potential of this approach owing to a better static description of spin and valence fluctuations. The importance of all the different aspects of the formalism has been analyzed in detail. This method is not to be looked at as an alternative to the earlier implementations within the LMTO-ASA band structure method. Its great potential, and in some way superiority, arises from the local and multiple scattering aspects through which the method lends itself easily to various generalizations and extensions on the account of the straightforward determination of the one-electron Green's function. Of particular interest here is an inclusion of dynamical fluctuations, for which a roadmap has been briefly outlined in the preceding section. The results of the present paper constitute the crucial steps on this road towards dynamics.

Finally, there is one more aspect of the present results which warrants further comment. As we have reported in Sec. VII G, in our DLM calculations local moment formed only when the local electronic structure was described by SIC-LSD, while it iterated to zero when LDA was used in recalculating the spin polarized crystal potential. This is precisely the behavior one would have expected on the basis of the numerous successes of SIC in predicting moment formation, and no moment formation in applications to extended systems.<sup>31,32</sup> Clearly, the fact that our local implementation of SIC, namely LSIC, behaves in this way lends strong support to our contention that self-interaction correction formalism can be, and perhaps should be, applied at the local level.

## ACKNOWLEDGMENTS

This work was partially funded by the EU Research Training Network (Contract No. HPRN-CT-2002-00295), *Ab-initio* Computation of Electronic Properties of *f*-electron Materials, and by the Deutsche Forschungsgemeinschaft through the Forschergruppe Oxidic Interfaces. Part of the

calculations were performed at the Rechenzentrum Garching, as well as the John von Neumann Institute for Computing in Jülich. Ole Krog Andersen is gratefully acknowledged for many useful and enlightening discussions over the years, and in particular those on a possible use of NMTOs in the full SIC-LSD implementation. Also Patrick Bruno is thanked for useful and stimulating discussions.

- 
- <sup>1</sup>J. P. Perdew and A. Zunger, Phys. Rev. B **23**, 5048 (1981).  
<sup>2</sup>R. A. Heaton, J. G. Harrison, and C. C. Lin, Phys. Rev. B **28**, 5992 (1983).  
<sup>3</sup>P. Strange, A. Svane, W. M. Temmerman, Z. Szotek, and H. Winter, Nature (London) **399**, 756 (1999).  
<sup>4</sup>A. Svane, W. M. Temmerman, Z. Szotek, L. Petit, P. Strange, and H. Winter, Phys. Rev. B **62**, 13 394 (2000).  
<sup>5</sup>W. M. Temmerman, H. Winter, Z. Szotek, and A. Svane, Phys. Rev. Lett. **86**, 2435 (2001).  
<sup>6</sup>L. Petit, A. Svane, Z. Szotek, and W. M. Temmerman, Science **301**, 498 (2003).  
<sup>7</sup>Z. Szotek *et al.*, Phys. Rev. B **68**, 054415 (2003).  
<sup>8</sup>R. Tyer *et al.*, Europhys. Lett. **65**, 519 (2004).  
<sup>9</sup>G. Banach and W. M. Temmerman, Phys. Rev. B **69**, 054427 (2004).  
<sup>10</sup>W. M. Temmerman, A. Svane, Z. Szotek, and H. Winter, in *Electronic Density Functional Theory: Recent Progress and New Directions*, edited by J. F. Dobson, G. Vignale, and M. P. Das (Plenum, New York, 1998), p. 327.  
<sup>11</sup>O. K. Andersen, Phys. Rev. B **12**, 3060 (1975).  
<sup>12</sup>P. Soven, Phys. Rev. **156**, 809 (1967).  
<sup>13</sup>G. M. Stocks, W. M. Temmerman, and B. L. Gyorffy, Phys. Rev. Lett. **41**, 339 (1978).  
<sup>14</sup>B. L. Gyorffy and G. M. Stocks, in *Electrons in Disordered Metals and at Metallic Surfaces*, edited by P. Phariseau, B. L. Gyorffy, and L. Scheire, NATO ASI Series Physics B42 (Plenum, New York, 1979).  
<sup>15</sup>J. S. Faulkner and G. M. Stocks, Phys. Rev. B **23**, 5628 (1981).  
<sup>16</sup>G. M. Stocks and H. Winter, in *The Electronic Structure of Complex Systems*, edited by P. Phariseau and W. M. Temmerman, NATO ASI Series Physics B113 (Plenum, New York, 1984).  
<sup>17</sup>J. Hubbard, Proc. R. Soc. London, Ser. A **276**, 238 (1963).  
<sup>18</sup>J. Hubbard, Proc. R. Soc. London, Ser. A **277**, 237 (1964).  
<sup>19</sup>J. Hubbard, Proc. R. Soc. London, Ser. A **281**, 401 (1964).  
<sup>20</sup>P. Hohenberg and W. Kohn, Phys. Rev. **136**, B864 (1964).  
<sup>21</sup>W. Kohn and L. J. Sham, Phys. Rev. **140**, 1133 (1965).  
<sup>22</sup>R. O. Jones and O. Gunnarsson, Rev. Mod. Phys. **61**, 689 (1989).  
<sup>23</sup>B. L. Gyorffy, A. J. Pindor, J. B. Staunton, G. M. Stocks, and H. Winter, J. Phys. F: Met. Phys. **15**, 1337 (1985).  
<sup>24</sup>J. B. Staunton, B. L. Gyorffy, G. M. Stocks, and H. Winter, J. Phys. F: Met. Phys. **16**, 1761 (1986).  
<sup>25</sup>A. Georges, G. Kotliar, W. Krauth, and M. J. Rosenberg, Rev. Mod. Phys. **68**, 13 (1996).  
<sup>26</sup>Y. Kakehashi, Phys. Rev. B **66**, 104428 (2002).  
<sup>27</sup>W. M. Temmerman, A. Svane, Z. Szotek, H. Winter, and S. Beiden, in *Electronic structure and Physical Properties of Solids: The Uses of the LMTO Method*, edited by H. Dreyssé, Lecture Notes in Physics No. 535 (Springer-Verlag, New York, 2000), p. 286.  
<sup>28</sup>S. L. Dudarev, A. I. Liechtenstein, M. R. Castell, G. A. D. Briggs, and A. P. Sutton, Phys. Rev. B **56**, 4900 (1997).  
<sup>29</sup>A. J. Pindor, W. M. Temmerman, and B. L. Gyorffy, J. Phys. F: Met. Phys. **13**, 1627 (1983); W. M. Temmerman and A. J. Pindor, *ibid.* **13**, 1869 (1983).  
<sup>30</sup>D. C. Koskenmaki and K. A. Gschneidner, Jr., in *Handbook on the Physics and Chemistry of Rare Earths*, edited by K. A. Gschneidner, Jr. and L. Eyring (North-Holland, Amsterdam, New York, Oxford, 1978), p. 337.  
<sup>31</sup>Z. Szotek, W. M. Temmerman, and H. Winter, Phys. Rev. Lett. **72**, 1244 (1994).  
<sup>32</sup>A. Svane, Phys. Rev. B **53**, 4275 (1996).  
<sup>33</sup>B. Johansson, I. A. Abrikosov, M. Aldén, A. V. Ruban, and H. L. Skriver, Phys. Rev. Lett. **74**, 2335 (1995).  
<sup>34</sup>N. Y. Moghadam *et al.*, J. Phys.: Condens. Matter **13**, 3073 (2001).  
<sup>35</sup>J. B. Staunton (private communication).  
<sup>36</sup>W. M. Temmerman, Z. Szotek, and H. Winter, Phys. Rev. B **47**, 1184 (1993).  
<sup>37</sup>D. M. C. Nicholson, G. M. Stocks, Y. Wang, W. A. Shelton, Z. Szotek, and W. M. Temmerman, Phys. Rev. B **50**, 14 686 (1994).  
<sup>38</sup>J. W. Allen and L. Z. Liu, Phys. Rev. B **46**, 5047 (1992).  
<sup>39</sup>B. Coqblin and A. Blandin, Adv. Phys. **17**, 281 (1968).  
<sup>40</sup>A. Svane, Phys. Rev. Lett. **72**, 1248 (1994).  
<sup>41</sup>I.-K. Jeong, T. W. Darling, M. J. Graf, T. Proffen, R. H. Heffner, Y. Lee, T. Vogt, and J. D. Jorgensen, Phys. Rev. Lett. **92**, 105702 (2004).  
<sup>42</sup>A. M. N. Niklasson *et al.*, Phys. Rev. B **67**, 235105 (2003).  
<sup>43</sup>J. L. Black and B. L. Gyorffy, Phys. Rev. Lett. **41**, 1595 (1978).  
<sup>44</sup>D. I. Cox and A. Zawadowski, *Exotic Kondo Effects in Metals* (Taylor and Francis, London, 1999).  
<sup>45</sup>M. Jarrell and H. R. Krishnamurthy, Phys. Rev. B **63**, 125102 (2001).  
<sup>46</sup>D. A. Rowlands, J. B. Staunton, and B. L. Gyorffy, Phys. Rev. B **67**, 115109 (2003).  
<sup>47</sup>D. A. Rowlands, J. B. Staunton, B. L. Gyorffy, E. Bruno, and B. Ginatempo, cond-mat/0411347, Phys. Rev. B (to be published).  
<sup>48</sup>K. Vladar, G. T. Zimanyi, and A. Zawadowski, Phys. Rev. Lett. **56**, 286 (1986).  
<sup>49</sup>D. R. Hamann, Phys. Rev. Lett. **23**, 95 (1969).  
<sup>50</sup>D. R. Hamann, Phys. Rev. B **2**, 1373 (1970).  
<sup>51</sup>The idea of a two-level system could, of course, be generalized to *N* levels.